Postprint for: Dastjerdi, Sh, Malikan, M., Akgöz, B, Civalek, Ö., Wiczenbach, T., Eremeyev, VA, On the deformation and frequency analyses of SARS-CoV-2 at nanoscale, INTERNATIONAL JOURNAL OF ENGINEERING SCIENCE.
DOI: 10.1016/j.ijengsci.2021.103604

On the deformation and frequency analyses of SARS-CoV-2 at nanoscale

Shahriar Dastjerdi [a], Mohammad Malikan [b], Bekir Akgöz [a], Ömer Civalek [c], Tomasz Wiczenbach [b], Victor A. Eremeyev [b, d, e, *]

[a] Division of Mechanics, Civil Engineering Department, Akdeniz University, Antalya, Turkey

[b] Department of Mechanics of Materials and Structures, Faculty of Civil and Environmental Engineering, Gdansk University of Technology, Gdansk, Poland

[c] Department of Medical Research, China Medical University Hospital, China Medical University, Taichung, Taiwan

[d] Research and Education Center "Materials" Don State Technical University, Gagarina sq., 1, 344000 Rostov on Don, Russia

[e] DICAAR, Università degli Studi di Cagliari, Via Marengo, 2, 09123, Cagliari, Italy
* Corresponding author:
victor.eremeev@pg.edu.pl

ABSTRACT

The SARS-CoV-2 virus, which has emerged as a Covid-19 pandemic, has had the most significant impact on people's health, economy, and lifestyle around the world today. In the present study, the SARS-CoV-2 virus is mechanically simulated to obtain its deformation and natural frequencies. The virus under analysis is modeled on a viscoelastic spherical structure. The theory of shell structures in mechanics is used to derive the governing equations. Whereas the virus has nanometric size, using classical theories may give incorrect results.

Consequently, the nonlocal elasticity theory is used to consider the effect of interatomic forces on the results. From the mechanical point of view, if a structure vibrates with a natural frequency specific to it, the resonance phenomenon will occur in that structure, leading to the destruction of the structure. Therefore, it is possible that the protein chains of SARS-CoV-2 would be destroyed by vibrating it at natural frequencies. Since the mechanical properties of SARS-CoV-2 are not clearly known due to the new emergence of this virus, deformation and natural frequencies are obtained in a specific interval. Researchers could also use this investigation as a pioneering study to find a non-vaccine treatment solution for the SARS-CoV-2 virus and various viruses, including HIV.

Keywords: SARS-CoV-2; Frequency analysis; Spherical structure; Viscoelastic property; Semi-analytical polynomial method.

1. Introduction

Coronaviruses are relatively old viruses that were first identified in 1874 as infectious bronchitis viruses in birds. At the beginning of the current century, the Coronavirus in East and West Asia was seen. Acute Respiratory Syndrome (SARS) infected more than 8000 people and killed 774 people between 2002 and 2003 (Weiss and Navas-Martin, 2005). In the following years, the Middle East Respiratory Syndrome Coronavirus (CoV-MERS or 2012-nCoV) became the cause of severe lower respiratory tract disease, which has spread to humans in the Middle East, causing 858 deaths 2494 infections (Assiri et al., 2013). In late 2019, a new coronavirus nominated as SARS-CoV-2, which causes a severe respiratory disease called Covid-19, appeared in Wuhan (Velavan and Meyer, 2020). Coronaviruses belong to the Coronaviridae family, SARS-CoV, MERS-CoV, and SARS-CoV-2 pathogens are found in this family. These viruses infect many mammals, including bats, dogs, gulls, wolves, and humans. All of these viruses lead to respiratory disorders of humans being. SARS-CoV-2 is an RNA

virus with approximately 80-160 nm and a genomic 27-35 kb size, which causes COVID-19 (Şahin, 2020). The viral infection is usually associated with upper respiratory tract inflammation, fever, headache, and cough. Infection with SARS-CoV and MERS-CoV can be asymptomatic in the early stages but can cause pneumonia, kidney failure, and even death in the later stages. The immune response is essential to controlling and fighting the coronavirus (Jin et al., 2020).

Furthermore, immune system dysfunctions can lead to immunopathology and death. A further understanding of how the immune system functions against the coronavirus can effectively control pneumonia. Chemotactic factors are essential for the immune response against the virus because they play a role in bringing leukocytes into the lungs (Stoll et al., 2018). Any change in these factors can cause the immune system to malfunction. Defects or abnormalities in the immune system can increase viral replication (Bansal et al., 2012). Moreover, if the immune system becomes overactive, it can damage tissues.

Since this virus has become a global problem, new and effective treatments are needed to improve patients and reduce its incidence. Of the most effective therapies for improving and treating this disease is using drugs with small molecular structures that usually work based on the inhibition of viral enzymes (Ma et al., 2012; Prajapat et al., 2020; Sirsi and Borden, 2014; Stoll et al., 2018). These include DNA and RNA polymerase, viral protein glycosylation, virus assembly, viral particle transport, virus release, and protease inhibitors to fight the virus, including antiviral drugs, anti-malarial drugs, anti-HIV drugs, anti-inflammatory drugs, and corticosteroids. Antiviral drugs use three mechanisms to counteract the virus, including inhibiting virus replication, inhibiting ion channels, and inhibiting serine protease. The therapeutic effect of drug chaperones, which promote the proper folding of proteins in the endoplasmic reticulum, is considered an endoplasmic reticulum stress reducer and suppresses

cellular dysfunction, inflammation, and apoptosis, and therefore represents a promising therapeutic strategy of Covid-19 (Aoe, 2019; Mirabelli et al., 2020).

Psychiatrists and medical professionals gradually turned their attention to vibration methods to create therapeutic and medical effects in medical practice, i.e., crushing kidney stones, psychiatry, physical therapy, and sports (Bills et al., 2019; Boyd-Brewer, 2003; Diniz et al., 2002; Fu et al., 2013). They may be utilized to transmit information among deaf people. Magnetic exciters can produce waves with a frequency of 1 to 100 Hz, which depending on the frequency type, can have excitatory or inhibitory effects. Low frequencies (less than or equal to 1 Hz) have inhibitory effects, and higher frequencies (more than 1 Hz) have stimulatory effects on neurons. There are many medical applications of low/high-frequency human treatment. Transcortical Magnetic stimulation (TMS) is a safe and non-invasive method that affects the stimulated area by sending magnetic waves to the cortical activity and making changes in the level of glucose and neurotransmitters' activity. Diathermy is a physiotherapeutic procedure consisting of local heating of tissues under the tension of a strong electromagnetic field, contributing to muscle relaxation and relieving pain sensations (de Kleer, 1986; Ziemann, 2004). Furthermore, the electromagnetic field finds particular application in oncology. One of the basic principles is radiotherapy, which irradiates the patient with radiation (e.g., X-rays or gamma rays) to reduce the tumor’s size and destroy cancer cells.

Additionally, electromagnetic waves are used in diagnostics. One of the best known is X-ray examinations (X-rays), which irradiate a specific body area with X-rays (Domenyuk et al., 2018). The same principle is also used for computed tomography and its more advanced form - positron emission tomography (PET), which detects and identifies neoplastic cells. Similar to computed tomography, magnetic resonance imaging (MRI) works with the difference that instead of x-rays, it employes radio waves and a magnetic field.

However, there is a lack of study of virus treatment using engineering methods, such as electromagnetic fields. Mirtskhulava et al. (1995) performed an investigation of mice with an intranasal injection of the H1N1 virus. They treated them with a 2 kHz pulsed electromagnetic field therapy (PEMF) at 1 μT, 10 μT, and 100 μT for 7 days within 30 minutes per day. Comparison to a control group has shown significant results. The control group virus titers increased from 800 to 3200 after three and five days, respectively. After the seventh day, the number falls to 1600. For comparison in the groups treated with PEMF, the number of virus cells after not all curation exceeded 400 and 800 for 10, 100 μT groups and 1 μT group, respectively.

Pica et al. (2006) performed a study on extremely low-frequency electromagnetic fields (ELF-EMF) and their influence on oncogenic viruses. In this study, Kaposi's sarcoma-associated with herpesvirus (KSHV or HHV-8) has been exposed to the effects of 1 mT, 50 Hz sine waves, for 24-72 h. After total exposure under ELF-EMF, the viral progeny was formed mainly consisting of defective viral particles.

Since Covid-19 is a novel viral infection, there are no effective prevention methods for spreading the virus. Currently, only vaccination and drugs are considered therapeutic strategies. On the other hand, Pawluk (2020) considers the excellent effect of PEMF as prevention in the incubation period and the last phase of COVID-19 infection - healing and repairing damaged tissues. Wierzbicki et al. (2021) investigated the resonant and transient harmonic vibrations of the Coronavirus family.

The absence of Covid-19 disease’s complete treatment and emergency medicine availability is now the main undergoing problem. The first approach to help infected people get healthy was to use a medicine invented for another virus, such as Ebola or HIV. A group of scientists at the Allergy National Institute and Infectious Diseases (US National Institutes of

Health) (de Wit, 2020) reported a small molecule-based drug called Remdesivir. The drug, previously formulated to treat Ebola, can successfully prevent and treat MERS in the monkey animal model. It was also reported positive results based on the drug's in vitro and in vivo trials on SARS and MERS. Accordingly, a clinical trial using the drug in 270 patients having Covid-19 was performed in China with mild to severe symptoms. As a result, this drug is mentioned as one of the appropriate medicines to reduce this virus's side effects. Another clinical study using this drug on 53 patients showed that this drug reduced oxygen demand in 68% of patients with Covid-19 (Grein et al., 2020).

Preliminary results (Beigel et al., 2020) of this clinical trial indicate that the use of a 10-day course of Remdesivir shows better clinical outcomes than placebo in the treatment of hospitalized patients with Covid-19. Favipiravir is the first approved new corona drug in China. Favipiravir showed mild side effects after clinical trials in people with Covid-19 (Dai et al., 2020).

Gautret et al. (2020) performed a clinical study on 42 patients with Covid-19, including 26 patients treated with hydroxychloroquine and 16 patients who did not take any medicine. Within six days of follow-up, the group that took the drug improved by 70%. Only when hydroxychloroquine is combined with azithromycin does it provide 100% improvement after six days.

Nowadays, careful analysis of mechanical behavior is essential to design and increase the reliability of nanostructures. Vibrations of nanostructures such as nanosheets are significant, and several theories and methods have been developed to explain the scale parameter on the vibrational behavior of nanosheets. Most classical theories of the mechanics of continuous environments are based on hyperelastic structural relationships that assume the stress at any point is a function of the strains at that point. The nonlocal theory first proposed by Eringen

states that the stress of any point is a function of the strain field of that point and a function of the strain of all continuous points in the media, see. (Eringen, 1983, 2002; Eringen and Edelen, 1972) and reference therein. In recent years, Eringen's nonlocal theory has been used to solve nanostructure problems. Examination of the results indicates that Eringen's theory of nonlocal elasticity has good accuracy. Compared with the classical theory of continuum mechanics, Eringen's approach can assume the large nanosized structures' behavior without many complicated equations. Eringen investigated the vibrational behavior of nanosheets using nonlinear continuous environment models. He also considered the small-scale effect by introducing a new parameter which is named the scale parameter. This theory has been extensively tested for the behavior of 1D nanostructures, i.e., nanorod, nanobeams, and carbon nanotubes subjected to bending, buckling, and vibration (Heireche et al., 2008; Murmu and Pradhan, 2009; Şimşek, 2011). What is more, accurate results prediction of nanostructures involves the small-scale effect consideration, as using local theories over-predicts the results.

According to the recent research mentioned in the literature review, there is no study on the frequency analysis of SARS-CoV-2 cells in nanoscale. The natural frequency of SARS-CoV-2 cells following Eringen's nonlocal elasticity theory is evaluated in this study. Furthermore, the governing equations are obtained by applying the shell theory of structures and considering the virus's body as a spherical structure. To get the natural frequencies of the SARS-CoV-2 virus, the derived dynamic equations are computed. Additionally, according to mechanics, the resonance phenomenon will occur at the natural frequencies of the structure. Moreover, it could cause the cell's protein chains to be destroyed. In this study, natural frequencies are investigated in a particular range due to the unknown mechanical properties of SARS-CoV-2. This study is preliminary and pioneering to achieve the non-vaccine medical treatment against viruses like the SARS-CoV-2 and, i.e., HIV.

2. Virus modeling

In this section, we will try to extract the governing equations of a spherical structure. In fact, the spherical geometric shape of the modeled state is a viral structure with a spherical appearance, which can be seen in Fig. 1. In the literature, there are some recent studies on the mechanical analysis of spherical shells (Audoly and Hutchinson, 2020; Sim et al., 2021; Yan et al., 2020; Yin et al., 2021). Fig. 1 shows the structure of the SARS-CoV-2 virus; the components can be seen in the figure. The geometric shape of the virus in Fig. 1 can be simulated with a very good approximation to a complete spherical structure in Fig. 2. In Fig. 2, the parameters $h, R,$ and k are the thickness, radius, and stiffness coefficient of the elastic foundation (simulated here as the effect of RNA on the deformation of the outer wall of the virus). The impact of the foundation is considered as a linear elastic spring. The governing dynamic equations can be obtained with a spherical viral model, which will be discussed in detail below.

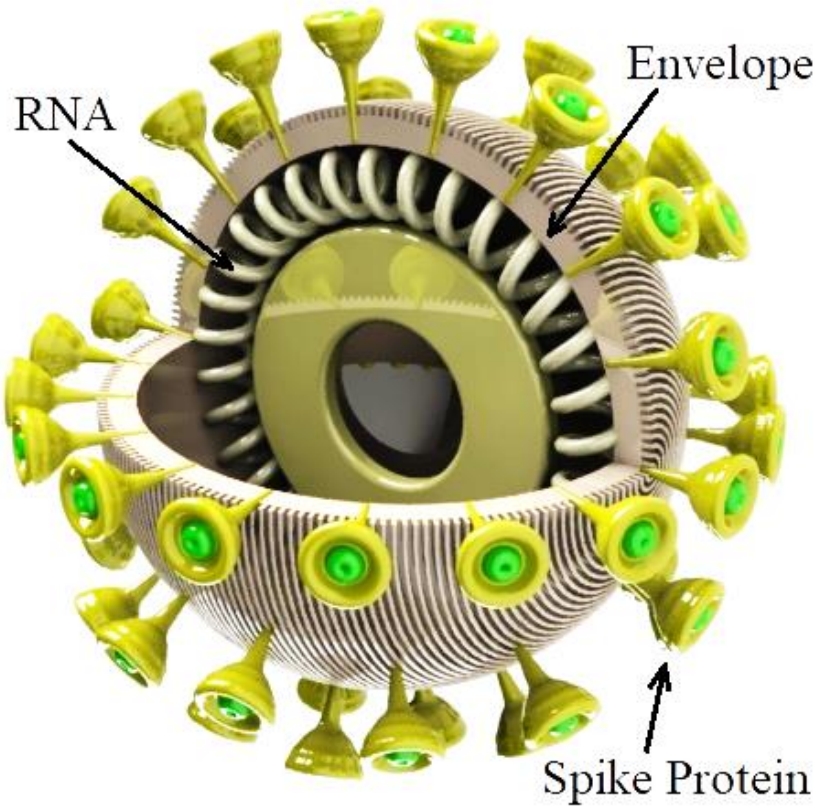

Fig. 1. Schematic view of SARS-CoV-2 virus

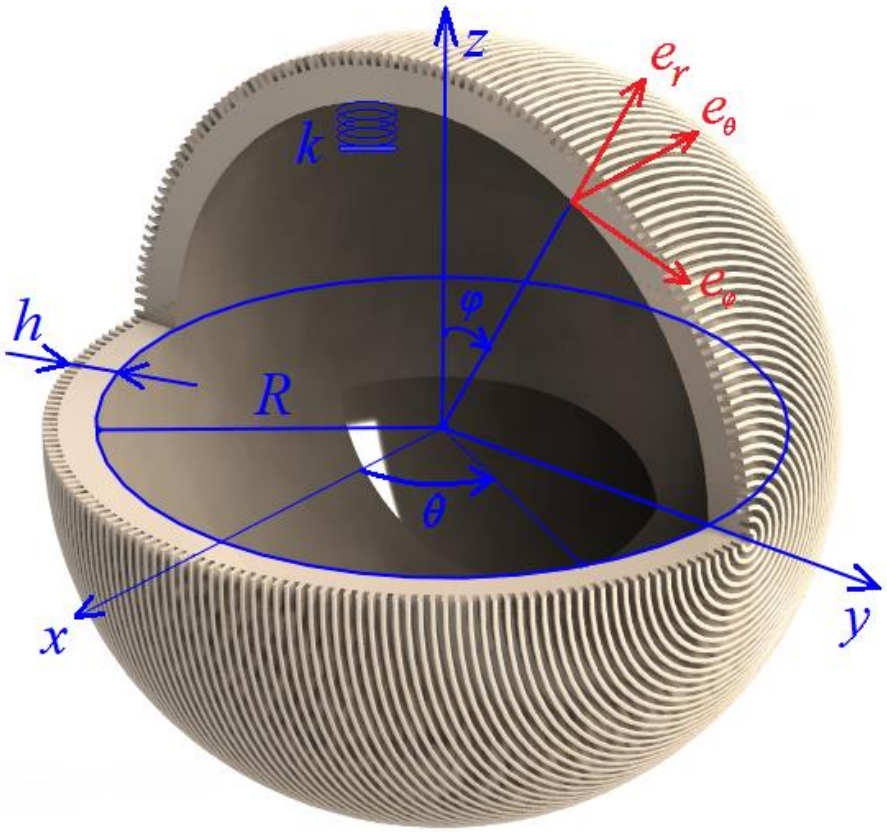

Fig. 2. Simulating the virus with a spherical structure and defining the coordinate system

3. Spherical coordinate system

Given that a spherical geometric shape model the viral structure, the best coordinate system that can be used to obtain the governing equations is the spherical coordinate system. In the spherical coordinate system, changes in the three principal directions r, φ, and θ are considered. The two spherical and Cartesian coordinate systems can be converted to each other with the following equations ($0 < \varphi < 180°, 0 < \theta < 360°$).

$$\begin{cases} x = r \sin\varphi \cos\theta \\ y = r \sin\varphi \sin\theta \\ z = r \cos\varphi \end{cases}$$

(1)

By performing mathematical calculations, the gradient vector according to the spherical coordinate system is introduced as the following equation.

$$\vec{\nabla}_{\text{Spherical}} = \left[\frac{\partial}{\partial r}\hat{e}_r \quad \frac{1}{R}\frac{\partial}{\partial \varphi}\hat{e}_\varphi \quad \frac{1}{R\sin\varphi}\frac{\partial}{\partial \theta}\hat{e}_\theta\right]$$

(2)

Given that the structure of the virus is entirely spherical ($\theta = 360°$) and also the properties of the constituent material are uniform, there will be no changes in the direction of θ. In addition, the displacement vector of an arbitrary point on the structure can be considered as the following equation.

$$\vec{U} = [U_r\hat{e}_r \quad U_\varphi\hat{e}_\varphi \quad U_\theta\hat{e}_\theta]$$

(3)

Also, the radius of the virus is considered to be approximately constant and equal to R, as a result, the change in the direction of r is equal to zero.

Consequently, it is observed that there will be only changes in the direction of φ, and therefore it is predicted that due to the existence of only one variable in the obtained equations, the differential equations are ordinary (without considering the time variable).

4. Stress and strain field

According to the definition of strain tensor as a general relation, the following components of strain tensor can be obtained for the structure of the virus according to the following equations.

$$\overleftrightarrow{\varepsilon} = \frac{1}{2}\left[\nabla\vec{U} + \nabla\vec{U}^T + \nabla\vec{U}\cdot\nabla\vec{U}^T\right]$$

(4)

$$\nabla\vec{U} = \begin{bmatrix} \frac{\partial}{\partial r}\hat{e}_r & \frac{1}{R}\frac{\partial}{\partial \varphi}\hat{e}_\varphi & 0 \end{bmatrix} \begin{bmatrix} U_r\hat{e}_r \\ U_\varphi\hat{e}_\varphi \\ 0 \end{bmatrix}$$

$$= \begin{bmatrix} 0 & \frac{\partial U_\varphi}{\partial r} & 0 \\ \frac{1}{R}\left(\frac{\partial U_r}{\partial \varphi} - U_\varphi\right) & \frac{1}{R}\left(\frac{\partial U_\varphi}{\partial \varphi} + U_r\right) & 0 \\ 0 & 0 & \frac{1}{R}\left(U_r + \cot\varphi\, U_\varphi\right) \end{bmatrix}$$

$$\overleftrightarrow{\varepsilon}_{ij} = \begin{bmatrix} \varepsilon_{rr} = 0 & \varepsilon_{r\varphi} & \varepsilon_{r\theta} = 0 \\ \varepsilon_{\varphi r} & \varepsilon_{\varphi\varphi} & \varepsilon_{\varphi\theta} = 0 \\ \varepsilon_{\theta r} = 0 & \varepsilon_{\theta\varphi} = 0 & \varepsilon_{\theta\theta} \end{bmatrix}$$

(5)

$$2\varepsilon_{r\varphi} = 2\varepsilon_{\varphi r} = \frac{\partial U_\varphi}{\partial r} + \frac{1}{R}\left(\frac{\partial U_r}{\partial \varphi} - U_\varphi\right)$$

$$\varepsilon_{\varphi\varphi} = \frac{1}{R}\left(\frac{\partial U_\varphi}{\partial \varphi} + U_r\right) + \frac{1}{2R^2}\left(\left(\frac{\partial U_r}{\partial \varphi}\right)^2 + U_r^2\right)$$

$$\varepsilon_{\theta\theta} = \frac{1}{R}\left(U_r + \cot\varphi\, U_\varphi\right) + \frac{1}{2R^2}(U_r)^2$$

Because the virus under consideration has a soft protein structure, the viscoelastic properties of the material have been assumed. It means that the strains on the structure are depended on time. There are several simulations for this aspect in mechanics; however, the Kelvin-Voigt model has been used in this research due to its efficient and straightforward formulation. The details for this consideration can be found in many papers (Dastjerdi and Abbasi, 2020; Dastjerdi et al., 2020, 2021a; Malikan and Eremeyev, 2020; Cruz-González et al., 2020; Ghayesh, 2019; Jalaei and Civalek, 2019). Eventually, the introduced strain components in Eq. (5) will be reformulated as follows (g and t represent the viscosity of the material and time respectively):

$$2\varepsilon_{r\varphi} = 2\varepsilon_{\varphi r} = \left(1 + g\frac{\partial}{\partial t}\right)\left(\frac{\partial U_\varphi}{\partial r} + \frac{1}{R}\left(\frac{\partial U_r}{\partial \varphi} - U_\varphi\right)\right) \tag{6}$$

$$\varepsilon_{\varphi\varphi} = \left(1 + g\frac{\partial}{\partial t}\right)\left(\frac{1}{R}\left(\frac{\partial U_\varphi}{\partial \varphi} + U_r\right) + \frac{1}{2R^2}\left(\left(\frac{\partial U_r}{\partial \varphi}\right)^2 + U_r^2\right)\right) \tag{7}$$

$$\varepsilon_{\theta\theta} = \left(1 + g\frac{\partial}{\partial t}\right)\left(\frac{1}{R}\left(U_r + \cot\varphi\, U_\varphi\right) + \frac{1}{2R^2}(U_r)^2\right) \tag{8}$$

Now that the strain tensor components are obtained, the stress tensor components can also be found according to Hooke's law ($\overleftrightarrow{\sigma_{ij}} = C : \overleftrightarrow{\varepsilon_{ij}}$). In the mentioned equation, matrix C represents the characteristic of the structure material, which is defined by the parameters of Young's modulus E and Poisson's ratio ν.

$$\begin{bmatrix}\sigma_{\varphi\varphi}\\ \sigma_{\theta\theta}\\ \sigma_{r\varphi}\end{bmatrix} = \frac{E}{(1-\nu^2)}\begin{bmatrix}1 & \nu & 0\\ \nu & 1 & 0\\ 0 & 0 & (1-\nu)\end{bmatrix}\begin{bmatrix}\varepsilon_{\varphi\varphi}\\ \varepsilon_{\theta\theta}\\ \varepsilon_{r\varphi}\end{bmatrix} \tag{9}$$

5. Nonlocal elasticity theory of Eringen

Whereas the SARS-CoV-2 virus size is analyzed at the nanometer scale, the existing classical theories can no longer be used for mathematical analysis and simulation (Kudin and Scuseria, 2001; Ivanovska et al., 2003; Eremeyev et al., 2015; Boni and Royer-Carfagni, 2021). For example, the above equation (which is Hooke's law of stress) represents local stresses. In other words, the stress at any point in the geometry range depends on the strain at that point. Eringen's theory of nonlocal elasticity has been used to obtain the governing equations in the present study. So many researchers due to its significant advantages (Dastjerdi and Akgöz,

2019; Dastjerdi et al., 2021b; Malikan et al., 2020a, b; Karami et al., 20219; Xu et al., 2021) have used the nonlocal elasticity theory widely. In nonlocal theory, the stress at a point on the geometry does not depend only on the strain at a similar point, but also on the amount of strain on the entire amplitude of the problem geometry. The differential form of the nonlocal elasticity theory is introduced according to the following equation.

$$[1-(e_0a)^2\nabla^2]\sigma_{ij}=\varepsilon_{ij} \qquad \mu=(e_0a)^2 \tag{10}$$

In the above equation, ∇^2 is the Laplacian operator that is introduced in the spherical coordinate system as $\nabla^2=\frac{1}{r^2\sin\varphi}\frac{\partial}{\partial\varphi}\left(\sin\varphi\frac{\partial}{\partial\varphi}\right)$ here. e_0 depends on the kind of material under study, which is a dimensionless parameter. Also, a is also a length-dependent parameter that depends on the factors affecting the analysis including geometric size, loading, boundary conditions, and environmental factors. Thus, the nonlocal parameter μ actually represents the intensity of the interatomic forces. The higher the numerical value of μ, the greater the effect of nanoscale analysis. Determining a specific value for a nonlocal parameter requires practical experiments. Therefore, according to the nature of this research which is a theoretical mechanics aspect, an interval from zero to a particular value has been considered for the nonlocal parameter (μ) which depends on the physical condition of the structure under analysis.

6. Governing equations

6.1. The principle of minimum potential energy

Earlier equations for nonlocal stress and strain tensors were introduced. It is now possible to obtain the governing dynamic equations by using the principle of minimum potential energy. In this method, the potential energy variations of the whole system must be equal to zero. The critical point of using this method is to obtain the dynamic governing equations with definitions

related to boundary conditions. Boundary conditions are of particular importance in mechanical science problems and, in fact, the physical description of the geometry boundaries. Different boundary conditions can be considered, each of which will create equations specific to those conditions. One of the most vital end conditions governing mechanical and physical phenomena is the free boundary condition. In other words, if the structure has no constraints on a geometric boundary and can move and rotate freely in all major directions, a free boundary condition will be created. The opposite of this description is the Clamp boundary condition, in which the freedom of transitional and rotational motion of the structure in all directions will be taken away.

The basic equation for the principle of minimum potential energy is according to the following equation in which $\delta U_{\varepsilon}, \delta U_{k}$ and δU_{ext} are variations of potential energy due to strain, kinetic and external forces on the structure, respectively.

$$\delta U_{Total} = \delta U_{\varepsilon} + \delta U_{k} + \delta U_{ext} = 0 \tag{11}$$

The potential energy variations for each component (strain, kinetic and external forces) will now be discussed and formulated separately. First, the strain energy variations (δU_{ε}) will be extended.

$$\delta U_{\varepsilon} = \int_{0}^{t} \left(\iiint_{V} \left(\sigma_{rr} \delta \varepsilon_{rr} + \sigma_{\varphi\varphi} \delta \varepsilon_{\varphi\varphi} + \sigma_{\theta\theta} \delta \varepsilon_{\theta\theta} + 2\sigma_{r\varphi} \delta \varepsilon_{r\varphi} \right) dV \right) dt \tag{12}$$

In the above integral equation applied to the volume of the structure (V refers to the volume of the structure), the expansion of Eq. (12) can be rewritten based on the nonlocal stresses and strains introduced in Section 3 as follows.

$$\delta U_{\varepsilon} = \int_0^t \left(\iiint_V \left(\sigma_{\varphi\varphi} \left(\frac{1}{R}\left(\frac{\partial \delta U_{\varphi}}{\partial \varphi} + \delta U_r \right) + \frac{1}{R^2}\left(\frac{\partial \delta U_r}{\partial \varphi} \right)\left(\frac{\partial U_r}{\partial \varphi} \right) \right) \right.\right.$$
$$+ \sigma_{\theta\theta} \left(\frac{1}{R}\left(\delta U_r + \cot\varphi\, \delta U_{\varphi} \right) + \frac{U_r \delta U_r}{R^2} \right)$$
$$\left.\left. + \sigma_{r\varphi} \left(\frac{\partial \delta U_{\varphi}}{\partial r} + \frac{1}{R}\left(\frac{\partial \delta U_r}{\partial \varphi} - \delta U_{\varphi} \right) \right) \right) R^2 \sin\varphi \, dr d\varphi d\theta \right) dt$$

(13)

The kinetic energy variation of the system with respect to the displacement vector $\vec{U}$ (which is only in the direction of φ) is introduced as the following equation.

$$\delta U_k = \frac{\delta}{2} \int_0^t \left(\iiint_V \rho \left(\left(\frac{\partial U_r}{\partial t} \right)^2 + \left(\frac{\partial U_{\varphi}}{\partial t} \right)^2 \right) dV \right) dt$$
$$= \int_0^t \left(\iiint_V \rho \left(\left(\frac{\partial U_{\varphi}}{\partial t} \frac{\partial \delta U_{\varphi}}{\partial t} \right) + \left(\frac{\partial U_r}{\partial t} \frac{\partial \delta U_r}{\partial t} \right) \right) R^2 \sin\varphi \, dr d\varphi d\theta \right) dt$$

(14)

Eventually, the potential energy variations due to external forces will be formulated. These external forces can be of various types, including distributed or concentrated loads, types of elastic and inelastic substrates, van der Waals forces, and so on. In this study, there will be the only uniform distributed transverse load applied to the inner or outer surfaces of the virus (inner or outer surface of the spherical geometry) as well as the elastic substrate simulated with a linear spring. The effect of the mentioned factors on the final extracted equations is considered in the following equation.

$$\delta U_{ext} = -\int_0^t \left(\iint_A \left(q_r(\delta U_r) - k(\delta U_r) \right) dA \right) dt \qquad (dA = R^2 \sin\varphi \, d\varphi d\theta)$$

(15)

6.2. Displacement field

So far, the displacement vector $\vec{U}$ has been introduced in a general form. Note that $\vec{U}$ is a three-variable function relative to the variables φ, r, and t (r is in the thickness direction). Three-variable function analysis will eventually lead to the extraction of partial differential equations. To facilitate calculations, the displacement vector can be introduced based on the displacement fields provided by the researchers so far. Of the most widely used and popular displacement fields is the first-order shear deformation theory (FSDT), which provides suitable results for moderately thick structures. Based on the FSDT displacement field, the shear force is defined linearly along with the structure thickness. As a result, a shear correction factor is used to modify the dissatisfaction of the zero shear force conditions at both the upper and lower surfaces of the structure ($r = \pm h/2$ in Fig. 2). In various studies, a specific value for this coefficient has been proposed, and its value is usually considered as $\kappa_s = 5/6$. The modified characteristic material matrix C that is defined in Eq. (9) will be reformulated by considering the value of κ_s as $C = \frac{E}{(1-\nu^2)}\begin{bmatrix} 1 & \nu & 0 \\ \nu & 1 & 0 \\ 0 & 0 & \kappa_s(1-\nu) \end{bmatrix}$. The displacement field according to FSDT theory is introduced according to the following equations for the displacement vector $\vec{U}$.

$$\begin{cases} U_\varphi(r,\varphi,t) = u(\varphi,t) + r.\psi(\varphi,t) \\ U_\theta(r,\varphi,t) = 0 \\ U_r(r,\varphi,t) = w(\varphi,t) \end{cases} \tag{16}$$

By placing the above equations in the energy equation (Eq. (11)), the variations in strain energy, kinetic energy, and external forces can be rewritten as the following equations.

$$\delta U_{\varepsilon} = \int_0^t \left(\int_{\theta_1}^{\theta_2} \int_{\varphi_1}^{\varphi_2} \int_{-\frac{h}{2}}^{\frac{h}{2}} \left(\sigma_{r\varphi} \left(\delta\psi + \frac{1}{R}\left(\frac{\partial \delta w}{\partial \varphi} - \delta u - r\delta\psi \right) \right) \right. \right.$$

$$+ \sigma_{\varphi\varphi} \left(\frac{1}{R} \left(\left(\frac{\partial \delta u}{\partial \varphi} + r\frac{\partial \delta \psi}{\partial \varphi} + \delta w \right) + \frac{1}{R} \left(\left(\frac{\partial \delta w_0}{\partial \varphi} \right) \left(\frac{\partial w_0}{\partial \varphi} \right) + w_0 \delta w_0 \right) \right) \right)$$

$$+ \sigma_{\theta\theta} \left(\frac{1}{R} \left(\left(\delta w_0 + \cot\varphi \left(\delta u_0 + r\delta\psi_1 \right) \right) \right. \right.$$

$$\left. \left. \left. + \frac{1}{R}\left(w_0 \delta w_0 \right) \right) \right) \right) R^2 \sin\varphi \, dr d\varphi d\theta \Bigg) dt$$

(17)

$$\delta U_k = \int_0^t \left(\iiint_V \rho \left(\left(\frac{\partial u}{\partial t} + r\frac{\partial \psi}{\partial t} \right) \left(\frac{\partial \delta u}{\partial t} + r\frac{\partial \delta \psi}{\partial t} \right) + \left(\frac{\partial w}{\partial t} \frac{\partial \delta w}{\partial t} \right) \right) dV \right) dt$$

$$= \int_0^t \left(\iint_A \left(I_1 \left(\frac{\partial u}{\partial t} \frac{\partial \delta u}{\partial t} \right) + I_2 \left(\frac{\partial u}{\partial t} \frac{\partial \delta \psi}{\partial t} + \frac{\partial \psi}{\partial t} \frac{\partial \delta u}{\partial t} \right) + I_3 \left(\frac{\partial \psi}{\partial t} \frac{\partial \delta \psi}{\partial t} \right) \right. \right.$$

$$\left. \left. + I_1 \left(\frac{\partial w}{\partial t} \frac{\partial \delta w}{\partial t} \right) \right) R^2 \sin\varphi \, dr d\varphi d\theta \right) dt \quad (I_1, I_2, I_3) = \int_{-\frac{h}{2}}^{\frac{h}{2}} \rho(1, r, r^2) dr$$

(18)

$$\delta U_{ext} = -\int_0^t \left(\iint_A \left(q_r(\delta w) - k(\delta w) \right) R^2 \sin\varphi \, d\varphi d\theta \right) dt$$

(19)

Now, by integrating into the direction of thickness r, the equations of strain energy variations can be made as equations as follows by considering the definitions related to stress and moment resultants.

$$\delta U_{\varepsilon} = \int_0^t \left(\int_{\theta_1}^{\theta_2} \int_{\varphi_1}^{\varphi_2} \left(N_{r\varphi}\delta\psi + \frac{1}{R}\left(N_{r\varphi}\frac{\partial \delta w}{\partial \varphi} - N_{r\varphi}\delta u - M_{r\varphi}\delta\psi \right) \right.\right.$$

$$+ \frac{1}{R}\left(N_{\varphi\varphi}\frac{\partial \delta u}{\partial \varphi} + M_{\varphi\varphi}\frac{\partial \delta\psi}{\partial \varphi} + N_{\varphi\varphi}\delta w \right.$$

$$+ \frac{1}{R}\left(N_{\varphi\varphi}\left(\frac{\partial w_0}{\partial \varphi}\right)\left(\frac{\partial \delta w_0}{\partial \varphi}\right) + N_{\varphi\varphi}w_0\delta w_0 \right)\Big)$$

$$+ \frac{1}{R}\left(\left(N_{\theta\theta}\delta w + \left(N_{\theta\theta}\delta u + M_{\theta\theta}\delta\psi \right)\cot\varphi \right) \right.$$

$$\left.\left.\left. + \frac{1}{R}\left(N_{\theta\theta}w_0\delta w_0 \right) \right) \right) R^2 \sin\varphi \, d\varphi d\theta \right) dt \tag{20}$$

$$\begin{cases} \left(N_{r\varphi}, N_{\varphi\varphi}, N_{\theta\theta} \right) = \int_{-\frac{h}{2}}^{\frac{h}{2}} \left(\sigma_{r\varphi}, \sigma_{\varphi\varphi}, \sigma_{\theta\theta} \right) dr \\ \left(M_{r\varphi}, M_{\varphi\varphi}, M_{\theta\theta} \right) = \int_{-\frac{h}{2}}^{\frac{h}{2}} \left(\sigma_{r\varphi}, \sigma_{\varphi\varphi}, \sigma_{\theta\theta} \right) r dr \end{cases} \tag{21}$$

Now, by adding similar terms of $\delta u, \delta\psi$ and δw, the nonlocal dynamic equations of the rounded spherical structure (virus shown in Fig. 1) will be derived as the following equations.

$$\delta u: -\left(\frac{\partial N_{\varphi\varphi}}{\partial \varphi} \right) + \cot\varphi \left(N_{\theta\theta} - N_{\varphi\varphi} \right) - N_{r\varphi} - R\left(I_1 \frac{\partial^2 u}{\partial t^2} + I_2 \frac{\partial^2 \psi}{\partial t^2} \right) = 0 \tag{22}$$

$$\delta w: -\frac{\partial}{\partial \varphi}\left(\sin\varphi \, N_{\varphi\varphi}\left(\frac{\partial w}{\partial \varphi} \right) \right) + \sin\varphi \, w\left(N_{\varphi\varphi} + N_{\theta\theta} \right) - \frac{\partial}{\partial \varphi}\left(R\sin\varphi \, N_{r\varphi} \right)$$

$$+ R\sin\varphi \left(N_{\varphi\varphi} + N_{\theta\theta} \right) - (q_r - k)R^2 \sin\varphi - R^2 \sin\varphi \left(I_1 \frac{\partial^2 w}{\partial t^2} \right) = 0 \tag{23}$$

$$\delta\psi: -R\sin\varphi\, M_{r\varphi} + R^2\sin\varphi\, N_{r\varphi} - R\frac{\partial}{\partial\varphi}\left(\sin\varphi\, M_{\varphi\varphi}\right) + R\sin\varphi\cot\varphi\, M_{\theta\theta}$$

$$- R^2\sin\varphi\left(I_2\frac{\partial^2 u_0}{\partial t^2} + I_3\frac{\partial^2\psi_1}{\partial t^2}\right) = 0$$

(24)

It is observed that the extracted equations are in nonlocal form. By applying the definition of nonlocal stresses (Eq. (10)) in the above equations and performing some mathematical calculations, the nonlocal parameter (μ) can be applied into the equations, and finally, a new form of equations in which there is a nonlocal parameter can be obtained according to the following equations.

$$\delta u: -\left(\frac{\partial N_{\varphi\varphi}}{\partial\varphi}\right) + \cot\varphi\left(N_{\theta\theta} - N_{\varphi\varphi}\right) - N_{r\varphi} - R(1-\mu\nabla^2)\left(I_1\frac{\partial^2 u}{\partial t^2} + I_2\frac{\partial^2\psi}{\partial t^2}\right) = 0$$

(25)

$$\delta w: R\left(N_{\varphi\varphi} + N_{\theta\theta} - \cot\varphi\, N_{r\varphi} - \frac{\partial N_{r\varphi}}{\partial\varphi}\right)$$

$$+ (1$$

$$- \mu\nabla^2)\left(\left(\left(\frac{\partial N_{\varphi\varphi}}{\partial\varphi}\right)\left(\frac{\partial w}{\partial\varphi}\right) + \cot\varphi\, N_{\varphi\varphi}\left(\frac{\partial w}{\partial\varphi}\right) + N_{\varphi\varphi}\left(\frac{\partial^2 w}{\partial\varphi^2}\right)\right.\right.$$

$$\left.\left. + w\left(N_{\varphi\varphi} + N_{\theta\theta}\right)\right) - (q_r - k)R^2 - R^2\left(I_1\frac{\partial^2 w}{\partial t^2}\right)\right) = 0$$

(26)

$$\delta\psi: -R\sin\varphi\, M_{r\varphi} + R^2\sin\varphi\, N_{r\varphi} - R\frac{\partial}{\partial\varphi}\left(\sin\varphi\, M_{\varphi\varphi}\right) + R\sin\varphi\cot\varphi\, M_{\theta\theta}$$

$$- R^2\sin\varphi\left(I_2\frac{\partial^2 u_0}{\partial t^2} + I_3\frac{\partial^2\psi_1}{\partial t^2}\right) = 0$$

(27)

The above equations are the final differential form of dynamic governing equations for the structure modeled in this research. According to the above equations, the deformations created in the structure which is under the transverse load of q_r and embedded in an elastic foundation with stiffness coefficient k, can be achieved in the two main directions of the displacement field U_φ and U_r.

However, the primary purpose of this study is to obtain the natural frequencies of the structure of Fig. 1. Mode frequencies can be determined according to the equations Eqs. (25-27). To obtain natural frequencies, the transverse load applied to the structure must be considered zero. The system response to the displacement field must be considered the following equations.

$$\begin{cases} U_\varphi(r,\varphi,t) = u(\varphi)e^{i\omega t} + r.\psi(\varphi)e^{i\omega t} = e^{i\omega t}\big(u(\varphi) + r.\psi(\varphi)\big) \\ U_r(r,\varphi,t) = w(\varphi)e^{i\omega t} \end{cases}$$

(28)

By applying the second derivative to the time of the above relations and given that ω is the natural frequency of the system, the terms $\frac{\partial^2 u}{\partial t^2}$, $\frac{\partial^2 \psi}{\partial t^2}$ and $\frac{\partial^2 w}{\partial t^2}$ will be obtained as follows.

$$\begin{cases} \dfrac{\partial^2 u}{\partial t^2} = -\omega^2 e^{i\omega t}u(\varphi) \\ \dfrac{\partial^2 \psi}{\partial t^2} = -\omega^2 e^{i\omega t}\psi(\varphi) \\ \dfrac{\partial^2 w}{\partial t^2} = -\omega^2 e^{i\omega t}w(\varphi) \end{cases}$$

(29)

By substituting the above equations (Eqs. (28, 29)) into the governing equations of the virus (Eqs. (25-27)), and considering $q_r = 0$ and neglecting nonlinear terms, the dynamic governing equations will be obtained to achieve the structure's natural frequencies as follows.

$$\delta u: -\left(\frac{\partial N_{\varphi\varphi}}{\partial \varphi}\right) + \cot\varphi\left(N_{\theta\theta} - N_{\varphi\varphi}\right) - N_{r\varphi} - R\omega^2(1-\mu\nabla^2)\left(I_1\frac{\partial^2 u}{\partial t^2} + I_2\frac{\partial^2 \psi}{\partial t^2}\right) = 0 \tag{30}$$

$$\delta w: R\left(N_{\varphi\varphi} + N_{\theta\theta} - \cot\varphi\, N_{r\varphi} - \frac{\partial N_{r\varphi}}{\partial \varphi}\right) + (1-\mu\nabla^2)\omega^2\left(kR^2 - R^2\left(I_1\frac{\partial^2 w}{\partial t^2}\right)\right) = 0 \tag{31}$$

$$\delta\psi: -R\sin\varphi\, M_{r\varphi} + R^2\sin\varphi\, N_{r\varphi} - R\frac{\partial}{\partial\varphi}\left(\sin\varphi\, M_{\varphi\varphi}\right) + R\sin\varphi\cot\varphi\, M_{\theta\theta}$$
$$- R^2\omega^2\sin\varphi\left(I_2\frac{\partial^2 u_0}{\partial t^2} + I_3\frac{\partial^2 \psi_1}{\partial t^2}\right) = 0 \tag{32}$$

It is observed that by solving the ordinary differential equations obtained, the frequency values ω can be obtained, and thus the frequency mode shapes for the viral structure of Fig. 1 will be calculated.

7. Boundary conditions

As mentioned earlier, using the principle of minimum potential energy simultaneously gives governing equations and a mathematical description of the boundary conditions. The mathematical description of the Free and Clamped boundary conditions is given in the following equations (φ_i and φ_f refers to initial and final boundaries in φ direction)

$$Clamped: u = \psi = w = 0 \qquad (\varphi = \varphi_i, \varphi_f) \tag{33}$$

$$Free: N_{\varphi\varphi} = N_{r\varphi} = M_{\varphi\varphi} = 0 \qquad (\varphi = \varphi_i, \varphi_f) \tag{34}$$

8. Solution methodology

In this research, there are two perspectives for solving the extracted equations, and the solution strategy is different for each one, which will be explained below:

1. Dynamic equations of the structure under distributed uniform transverse load (bending analysis).
2. Dynamic equations of structure to obtain natural frequencies.

To obtain the structural deformations of the virus according to Eqs. (25-27), the SAPM solution method previously proposed by the authors of this study can be used effectively (Dastjerdi et al., 2021c). Details of this method can be seen in previous research (Dastjerdi and Akgöz, 2019, 2020). According to the SAPM, the system of differential equations is transformed into a system of algebraic equations by using polynomial functions that can be easily solved by applying numerical solution methods. Finally, the unknowns of the problem (which are the displacement field functions) will be obtained. As a result, other unknowns can be achieved by specifying the displacement field parameters.

The second case is considered to be that the transverse load applied to the system is zero, and natural frequencies must be obtained. The eigenvalue problem is attended in which eigenvalues are, in fact, the natural frequencies of the system. One of the efficient numerical methods that have been highly regarded by researchers and can be used to analyze eigenvalue problems (natural frequency and buckling analyzes) is the differential quadrature method (DQM) (Li et al., 2021). In this numerical method (for solving differential equations), a weight function can be introduced for any value of first, second, etc., derivatives. Unlike the Finite Difference (FD) solution method, where the derivative at a specific point depends on the numerical values of the points before and after, in the DQM method, this range is wider, and the derivative at a particular point depends on the numerical value in the whole network of

problem geometry. Of course, the effect of closer points is greater, and, as mentioned, this effect is determined by the weight function. Second-order, third-order, and higher-order derivatives can be extracted according to the obtained first-order derivative. For example, for a one-dimensional problem that changes in the direction of x in the range x_1 to x_N (N represents the number of nodes) is considered. The derivative of N^{th}-order is introduced by the following equations.

$$\left.\frac{d^{(n)}f}{dx^{(n)}}\right|_{x_i} = \sum_{j=1}^{N} A_{ij}^{(n)} f(x_i) \qquad (i = 1..N) \tag{35}$$

$$A_{ij}^{(n)} = n\left(A_{ij}^{(1)} A_{ii}^{(n-1)} - \frac{A_{ij}^{(n-1)}}{(x_i - x_j)}\right) \qquad i \neq j,\ A_{ii}^{(n)} = -\sum_{j=1, \neq i}^{N} A_{ij}^{(n)} \qquad i,j = 1..N \tag{36}$$

In the analysis of the virus structure, the 4^{th}-order derivatives must be calculated for some displacement field functions. By deriving derivatives using DQM functions numerically, these values can be substituted into the governing equations. By substituting Eqs. (35, 36) into Eqs. (30-32), the differential equations will be discretized into a system of algebraic equations. As a result, an eigenvalue problem will be obtained as $([K] - \omega^2[M])[D] = 0$. $[D]$ is actually the displacement matrix at the nodes of the problem geometry domain. Also, $[K]$ and $[M]$ are the stiffness and mass matrixes, respectively. For example, if the number of $N = 9$ nodes in the structure's geometry is considered in the direction of φ, the matrix $[D]$ will be introduced as follows (T is the transpose of the matrix).

$$D^T = [u_1 \quad u_2 \cdots u_9 \quad \psi_1 \quad \psi_2 \cdots \psi_9 \quad w_1 \quad w_2 \cdots w_9]_{1\times 27} \tag{37}$$

$$\beta = [K] - \omega^2[M] = \begin{bmatrix} \beta_{11} & \cdots & \beta_{1(27)} \\ \vdots & \ddots & \vdots \\ \beta_{(27)1} & \cdots & \beta_{(27)(27)} \end{bmatrix} \tag{38}$$

By calculating the determinant of the matrix β as $|\beta|$ and setting it to zero, a characteristic equation of degree N will be obtained. By numerically solving this equation (which is only unknown ω), the first mode frequency up to $3 \times N^{th}$ mode number will be obtained.

Lower frequency modes are usually more important. Because such frequencies are more likely to occur. Therefore, in this research, the first and second modes will be discussed more than others. By changing the parameters affecting the problem, natural frequencies can be calculated in any desired condition. Factors such as virus size (radius R), thickness (h), elastic stiffness coefficient value (k) as well as the value of the nonlocal parameter of nanoscale analysis (μ) can be studied on the results. Therefore, the effect of each mentioned parameter on the results will be studied individually.

9. Numerical analysis and review of essential parameters

9.1. Evaluation of results

Before examining the effect of important factors, one must make sure that the obtained results are correct and accurate. For this purpose, a comparison between the obtained results in this study and previous research and a comparison with the results of existing popular software will be made. To evaluate a spherical structure with the following geometric and physical characteristics is considered.

$$R = 1.15\ m, h = 0.02\ m, E = 190\ GPa, \nu = 0.29, \varphi_i = 10°, \varphi_f = 170° \tag{39}$$

Now, the natural frequencies of the considered structure can be compared with the obtained results from ABAQUS software. Also, in the first part of solving the obtained dynamic equations, the SAPM method was applied to analyze the structure that is under a uniform transverse load (bending analysis). Therefore, the deformation results of the structure can be compared with the results of ABAQUS software. In general, the comparisons of bending and

frequency analyses can be seen in Figs. 3a, b, and Table 1 respectively (B.C. refers to the type of boundary conditions). The frequency comparison has been presented for two types of Clamped-Clamped (CC) and Free-Clamped (FC) boundary conditions at φ_i and φ_f edges. As can be seen, the achieved results from the mechanical modeling method performed in this study are slightly different from the results of ABAQUS software. ABAQUS is a very popular and accurate finite element software that has been used widely by mechanical engineers and researchers. Therefore, the simulation performed in the present study is reliable, and its consequence results can be used with sufficient confidence. In the following, the effect of the factors affecting the results (which were mentioned earlier) will be examined. It is aimed to examine the factors that have the greatest impact on the results in practice.

Table 1. Comparison between the first natural frequency results of this paper and ABAQUS software

	First natural frequency (kHz)							
B.C.	$R/h = 100$		$R/h = 50$		$R/h = 20$		$R/h = 10$	
	Paper	ABAQUS	Paper	ABAQUS	Paper	ABAQUS	Paper	ABAQUS
CC	0.465	0.472	0.930	0.944	2.335	2.369	4.733	4.793
FC	0.270	0.275	0.541	0.550	1.362	1.382	2.788	2.826

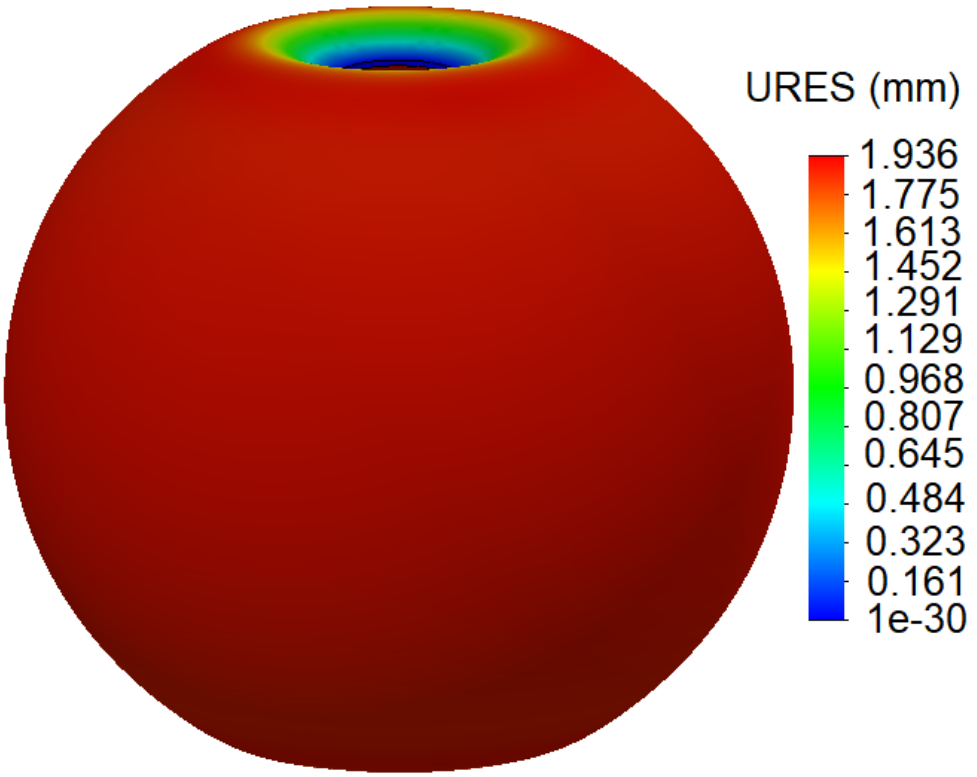

(a)

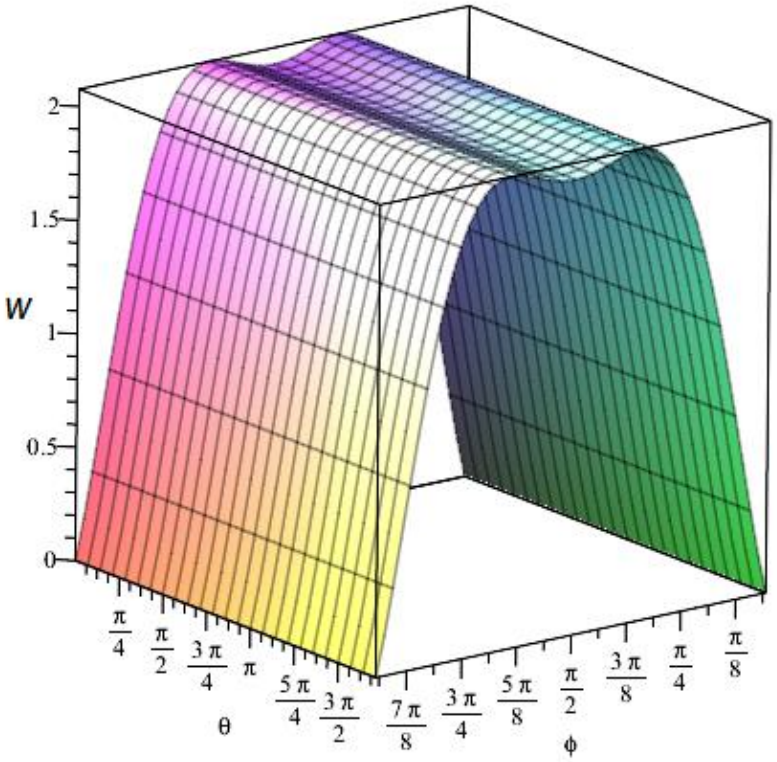

(b)

Fig. 3. Deflection w (mm) results of (a) ABAQUS software (b) present paper

9.2. Investigating the effect of essential factors on the results

Due to the viscoelastic properties of the structure of the SARS-CoV-2 virus, it is possible to plot the deformations created in it according to the passage of time. Fig. 4 shows the time-related changes in the mentioned deformations for different values of the parameter g, which in fact represents the viscosity of the virus material. It is observed that the deformation created in the virus increases with increasing time. The slope of the changes in Fig. 4 is highly dependent on the value of g, and these changes are nonlinear with decreasing slope. In Fig. 4, $g = 0$ indicates the state that the structure strains are not time-dependent, and it can be concluded that as soon as the load is applied, the maximum final deformation occurs in the structure. However, the higher the value of g, the longer it will take for maximum deformation to occur. Eventually, over time (increasing t on the horizontal axis), all the graphs will converge to a certain value, which here is about $4.75\ nm$. The duration of the applied loading can have a significant effect on the deformation of the virus. Since it may not be possible to determine a specific value for virus viscosity to be analyzed, it is recommended to apply the load for a more extended period of time to maximize deformation. In the performed calculations related to Fig. 4, a specific value of 0.75 is assumed for the nonlocal parameter $(e_0 a)/h$. In order to investigate the effects of nanoscale analysis, the changes of $(e_0 a)/h$ on the results should be studied, which will be discussed in continue.

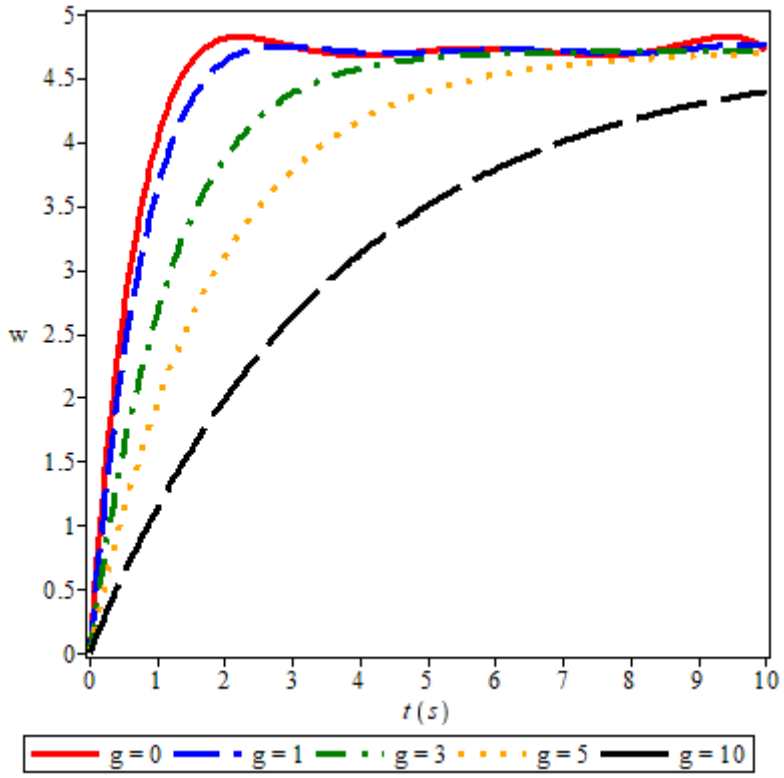

Fig. 4. Variations of deflection (nm) due to time for different values of viscosity g ($N.s/m^2$)

In the rest of the analysis, the mechanical properties of the virus are used regarding Table 2 (Stephanidis et al., 2007).

Table 2. Mechanical properties of the virus

$E(GPa)$	υ	$\rho(kg/m^3)$
3	0.3	1.2

The effect of nanoscale analysis on the results of deformation in the virus will now be examined. As can be expected, the smaller the structure at the nanoscale, the greater the effects of the atomic forces, which are simulated by the nonlocal parameter. Therefore, the mentioned explanation should also be considered (the radius of the virus, which indicates its size). The radius of the SARS-CoV-2 virus does not have a specific value, and an interval can be considered for it. The range for the virus radius in this study is between $50 < R < 120$ (nm).

Fig. 5 shows the deformations of the virus against the dimensionless nonlocal parameter changes. Changes have been examined for different values of virus radius. The stiffness coefficient of the elastic foundation (the effect of reaction forces caused by the internal materials of the virus such as RNA) is considered equal to $K = 10\ GPa/nm^2$. It is observed that at the beginning of the changes, the deformation is approximately the same for different values of the virus radius ($(e_0 a)/h = 0$). The slope of the changes is initially small and almost zero. But gradually, with increasing the nonlocal parameter, the slope of changes increases. In other words, the nonlocal parameter will affect the reduction of virus deformation. It can be understood that by increasing the nonlocal parameter, the effect of interatomic forces increases, and physically it can be described that the strength of the structure increases. Of course, determining the exact value of the nonlocal parameter is a fundamental challenge, and only by performing experimental efforts, the exact value of the nonlocal parameter can be obtained. It should be noted that the experimental values for $(e_0 a)$ are obtained only for specific conditions of the same problem, and by changing the parameters, different values will be obtained. Also, as can be expected earlier, the effects of nanoscale analysis are reduced by increasing the radius of the virus. For example, in the range $0 < \frac{(e_0 a)}{h} < 10$, a reduction of about 100% is observed for a virus with a radius of $R = 50\ nm$, which results in a reduction of about 30% for a virus with a radius of $120\ nm$. Therefore, if the radius of the virus is assumed to be about $100\ nm$, due to the unknown value of the nonlocal parameter $(e_0 a)$, we can use the results of classical analysis ($(e_0 a) = 0$) instead of the nonlocal analysis, which has simpler and fewer computational equations.

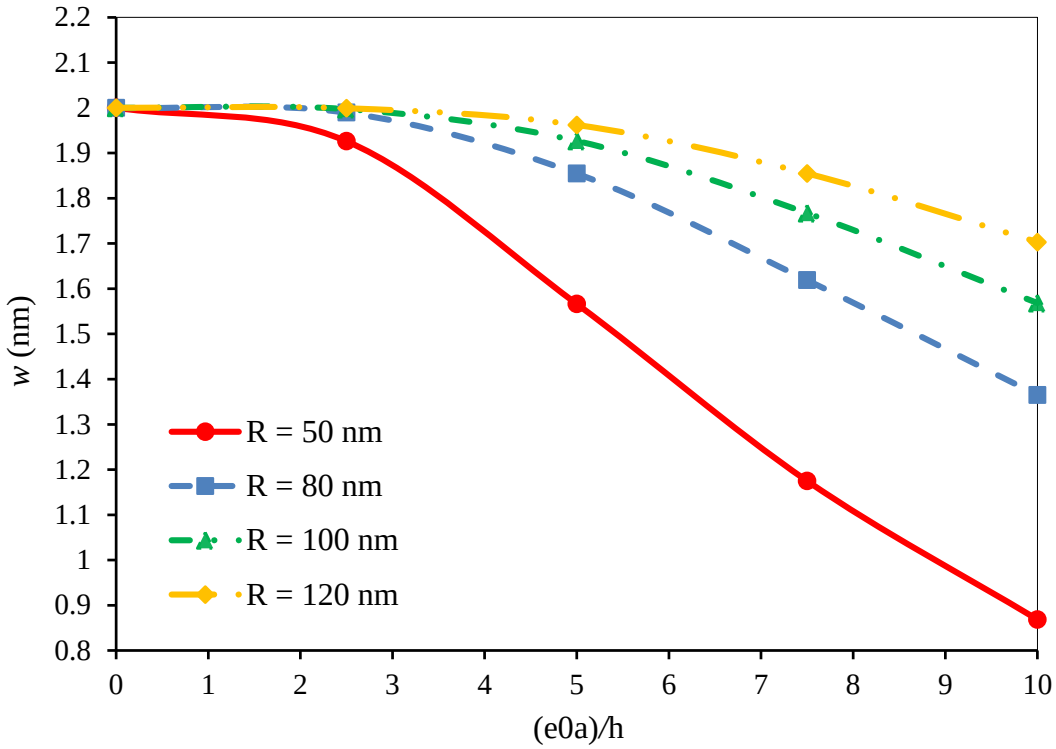

Fig. 5. Deflection results versus the dimensionless nonlocal parameter $(e_0a)/h$ for different values of virus radii

In the calculations performed in Fig. 5, as mentioned, the amount of elastic substrate stiffness is assumed $K = 10\ GPa/nm^2$. However, determining a specific value for K is also a challenge that can only be achieved by experimental works. Therefore, K changes can also be examined on the results. Fig. 6 shows the virus deformation in exchange for increasing the value of K for different values of the dimensionless nonlocal parameter $(e_0a)/h$. The amount of dimensionless deformation w_n is the ratio of nonlocal to classical deformation results. It is observed that the changes are decreasing, and at first, the slope of the graphs is very steep. And for a value of K onwards there is no noticeable change in w_n. The higher the (e_0a) value, the greater the distance between nonlocal and classical results. For example, for $\frac{(e_0a)}{h} = 2.5$, the results of both local and nonlocal analyzes are approximately the same. But for the mentioned

result, for $\frac{(e_0 a)}{h} = 10$, about 20% of the difference between local and nonlocal results is observed. In Fig. 5, the value assumed for K is vast, and it can be concluded that the effective interval for applying K to the results is $0 < K < 0.1$ (GPa/nm^2). In other words, considering the value of $K = 10\ GPa/nm^2$ with the state that $K = 1\ GPa/nm^2$ will not make much difference in the results. In the calculations performed in Fig. 6, the virus radius is assumed to be equal to $100\ nm$. One can see the dimensionless deformation changes w_k (the ratio of the amount of deformation in the case where there is an elastic foundation and its stiffness coefficient equal to K to the deformation of the structure without the presence of an elastic substrate) due to changes of K for different values of the virus radius in Fig. 7. The results described in Fig. 7 are almost similar to Fig. 6. It is observed that as the radius of the virus increases, the slope of the changes will increase. In other words, the effect of the elastic foundation for the virus with larger radii will be more intense. As a result, it further reduces the deformation of the virus. Of course, the difference between the results for different values of K will not be significant. Especially as the radius of the virus increases, the distance between the results decreases. For example, by increasing the radius of the virus from 50 to $80\ nm$, the difference between the obtained deformations is noticeable. However, by increasing the radius of the virus, the difference between the results can be ignored. In general, one can conclude that the larger the radius of the virus, the greater the effect of the internal material under the virus wall (which is assumed to be an elastic foundation) to reduce its deformation. As a result, a stronger load shall be imposed on the virus to create the intended deformation. If the structure of the SARS-CoV-2 virus is assumed to be without an elastic foundation, the deformations created in it will be much greater. Nevertheless, in reality, this is not the case, and internal materials affect the deformation and thus reduce it.

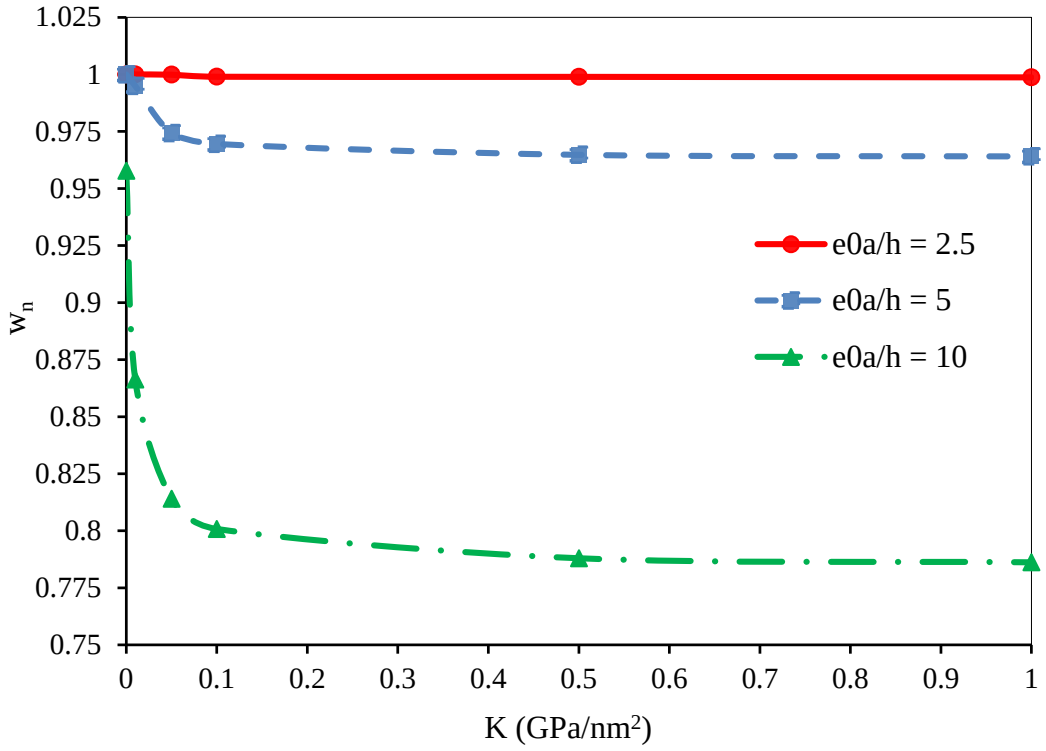

Fig. 6. Dimensionless deflection w_n versus K variations for different values of dimensionless nonlocal parameter $(e_0 a)/h$

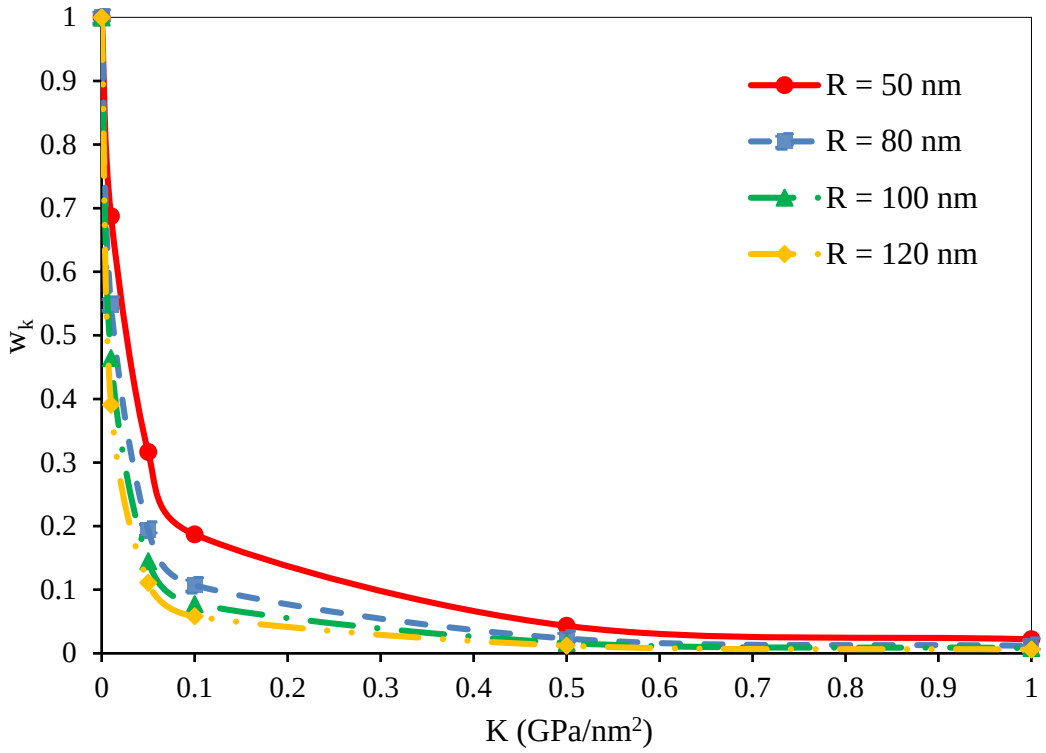

Fig. 7. Dimensionless displacement results versus stiffness coefficient of elastic foundation *K* for different values of virus radii

In Figs. 4 to 7, the effect of parameters on the deformation results in the virus wall has been investigated. Applying force to a structure can cause it to break mechanically. Here, because it is a viral structure that is replicating in the human body or an organism, it is mechanically possible to apply force to it, although it is complicated in practice. However, innovative solutions can also be considered for this purpose. In addition to applying mechanical load, frequency analysis can also be used as a solution to destroy the structure of the virus. According to mechanics, if a structure vibrates at its natural frequency, a resonance phenomenon will occur, which in practice can cause the structure to vibrate with extreme amplitudes. In other words, if the natural frequencies of the virus that the human body is infected with and due to which the disease is caused can be calculated. After that, the body exposed to these specific frequencies (according to the type of first, second, or higher natural frequencies),

the virus structure can be expected to vibrate with very large amplitudes. In the meantime, the protein structure of the viruses may break down, and the virus may destroy. These waves can even be used to break the protein chain within the virus. Therefore, it is crucial to obtain the natural frequencies of the structure of the SARS-CoV-2 virus. This method is not limited to eliminating the virus and can be used to kill other types of viruses such as HIV or even a variety of tumors and cancer cells that have a microscopic and macroscopic scale. Of course, it should be reminded that if the human body is exposed to such waves, it must not be dangerous or harmful to other organs or vital enzymes in the body. Even this treatment must not affect the human DNA and the risk of transmission to future generations. Indeed, if this mechanical concept is used as a treatment method, specialist physicians should make clinical considerations. Therefore, the purpose of this study is only to present a theoretical assessment regarding the elimination of the virus structure by applying force or frequency.

Due to the viscoelastic properties of SARS-CoV-2 virus material, this issue should be investigated in response to the natural frequencies of the virus. In Table 3, the first natural frequency is calculated for different values of viscosity and dimensionless nonlocal parameter $(e_0 a)/h$. It is observed that with increasing value g, the obtained natural frequency increases. Also, the increase in natural frequency will occur in return for the increase in the dimensionless nonlocal parameter $(e_0 a)/h$. This conclusion means that if the effects of nonlocal analysis increase, the distance between the nonlocal and classical results will be intensified. The effect of viscoelasticity on f_1 is more remarkable for larger values of $(e_0 a)/h$. For low viscosity values, the natural frequency values of f_1 can be used with a suitable approximation, regardless of the viscoelastic property. This is more evident for small nonlocal parameter values. It tends to be anticipated that if the range of the virus is about $100\ nm$, the effects of nonlocal analysis on f_1 are small. Therefore, for these types of viruses, the first natural frequency can be

considered with a suitable approximation, in which only the effects related to viscosity are considered.

Table 3. The effect of dimensionless nonlocal parameter $\frac{(e_0 a)}{h}$ and viscosity g on the first natural frequency of SARS-CoV-2 virus

$g\ (Pa.s)$	f_1		
	$\frac{(e_0 a)}{h} = 0$	$\frac{(e_0 a)}{h} = 5$	$\frac{(e_0 a)}{h} = 10$
0	3.308	3.568	4.758
1	3.510	3.805	5.186
5	4.427	4.891	7.221
10	5.767	6.503	10.322

In this research, only the effect of essential parameters on the results of the first and second modes of natural frequencies have been considered and investigated. In Figs. 8a and b, we can see the changes in the natural frequencies of the first and second modes in exchange for increasing the dimensionless nonlocal parameter $(e_0 a)/h$ for different values of the virus radius. The first result, according to Figs. 8a and b, as the virus's radius increases, the first and second natural frequencies will decrease. In other words, the larger the structure size, the lower the natural frequency required to occur resonance. Fig. 8a shows that f_1 increases with rising the nonlocal parameter (actually increasing interatomic forces). It is seen, the process of change for $R = 50\ nm$ is slightly different from other radii of the virus. Initially, the frequency changes of the first mode are incremental ($\frac{(e_0 a)}{h} = 7.5$) and then for $\frac{(e_0 a)}{h} > 7.5$, it is observed that the first natural frequency decreases. But for virus radii in the range $80\ nm < R\ < 120\ nm$, the trend is similar. As the radius of the structure increases, the effects of interatomic forces are observed to decrease. It is also observed that in the range $0 < \frac{(e_0 a)}{h} < 7.5$ the slope of changes is gentle and then the slope increases. The mentioned result is more evident for the radius of

80 nm. For a virus with a radius of about 100 nm, it can be observed that for the first natural frequency 3 $GHz < f_1 < 4\ GHz$, a resonance phenomenon will occur. However, this range for a virus with a radius of 50 nm is between 6 and 13 GHz. The SARS-CoV-2 virus usually has a radius of about 100 nm. Therefore, the interval for f_1 is considered smaller. The mentioned results for the second natural frequency (f_2) can also be seen in Fig. 8b. Here there are fluctuations in variations of the second natural frequency results. There is a peak for f_2 due to the increase of the dimensionless nonlocal parameter $(e_0 a)/h$. It is observed that by increasing the radius of the virus, the peak will be seen for larger values of $(e_0 a)/h$. Only the trend of changes in f_2 for a radius of 150 nm will be similar to the trend of changes in f_1. The natural frequency of f_2 is higher than f_1, and it can be concluded that the effects of nanoscale analysis on f_2 are greater than f_1. The range of frequency changes (f_2) for a virus with a radius of 100 nm will be between 7 $GHz < f_2 < 25\ GHz$. The resulting interval for f_2 is greater than f_1. From a practical perspective, the specimen will reach the first natural frequency. Therefore, because the nonlocal frequency range for f_1 is less than f_2, it is more likely to reach the first nonlocal natural frequency. This result is because determining the value of a nonlocal parameter is theoretically possible in only one interval, and the fewer changes in this interval, the more accurate the exact result can be achieved.

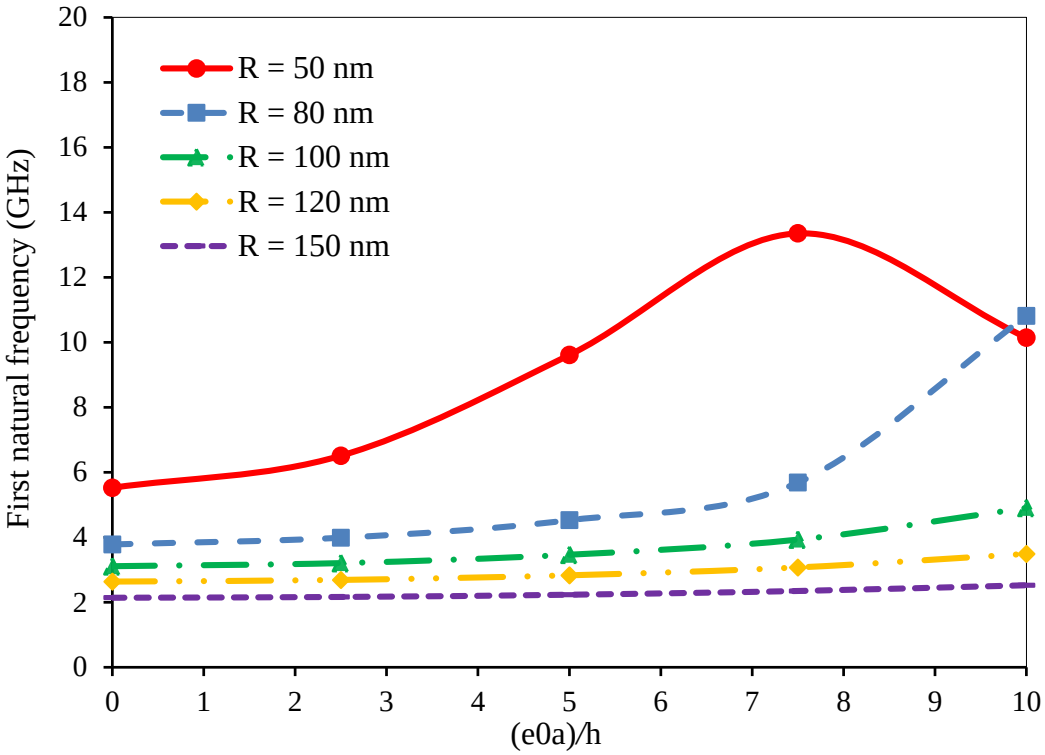

(a)

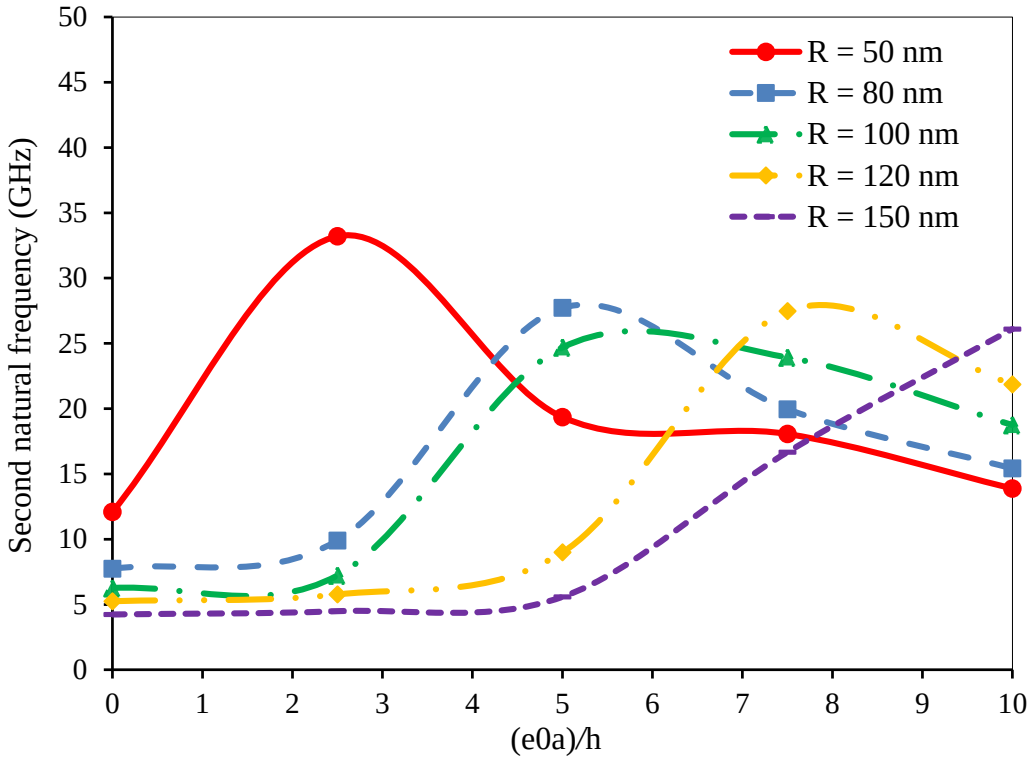

(b)

Fig. 8. Results due to dimensionless nonlocal parameter for different values of virus radii (a) first (b) second natural frequency

As mentioned earlier, the effect of internal materials of the SARS-CoV-2 virus (which is simulated in this study as an elastic substrate) on the deformation and natural frequency results is very high. Therefore, it is possible to observe the first and second dimensionless natural frequency changes against the changes of the elastic stiffness coefficient K in Figs. 9a and b. Graphs are plotted for different nonlocal parameter values. Fig. 9a shows that for $\frac{(e_0 a)}{h} = 0$, increasing the value of K (only slightly) will cause a sharp drop in the first natural frequency. The lower the nonlocal parameter value, the lower the result and the sharper the f_1 frequency drop. Then, after a sharp drop in f_1, with increasing the value of K, no significant change in f_1 results is observed. The dimensionless frequency f_1 is, in fact, the ratio of the obtained nonlocal natural frequency (for a given value of the nonlocal parameter) to the classical natural frequency ($\frac{(e_0 a)}{h} = 0$). As shown in Fig. 8, increasing the value of $(e_0 a)/h$ increases the natural frequency compared to the classical analysis (of course, in the case of the second natural frequency, there is fluctuation in the results and cannot be said with certainty in all acquired conditions). The results will now be reviewed in Fig. 9a. A sharp drop in the first natural frequency (Fig. 9a) means that for $\frac{(e_0 a)}{h} = 10$, an increase in the stiffness of the elastic foundation will bring the two nonlocal and classical analyzes closer together. Therefore, if it can be concluded from experimental works that the value of K is significant, the results of the classical analysis can be used. Because, as stated earlier, determining a specific value for the nonlocal parameter is a tough challenge in the nonlocal elasticity theory. According to Fig. 9a, the lower the $(e_0 a)/h$ value, the closer the results of the classical and nonlocal analyzes are. Fig. 9b gives the same results as for Fig. 9a, except that for the second natural frequency. The results of the classical and nonlocal analyses are more distant from each other. For example, in Fig. 9a, with a slight

increase in K, the distance between the classical and nonlocal results approaches each other with a growth of about 125%. However, the same result in Fig. 9b will be only about 20%. Therefore, in the case of f_2, even an increase in K has little effect on the approach of the classical and nonlocal analyzes. Therefore, if resonance is to be achieved by vibrating the SARS-CoV-2 virus at the second natural frequency (f_2), the nonlocal analysis must be used to make the resonance phenomenon more confident. Determining the K value for this nanometer-sized virus is a very complex and challenging task.

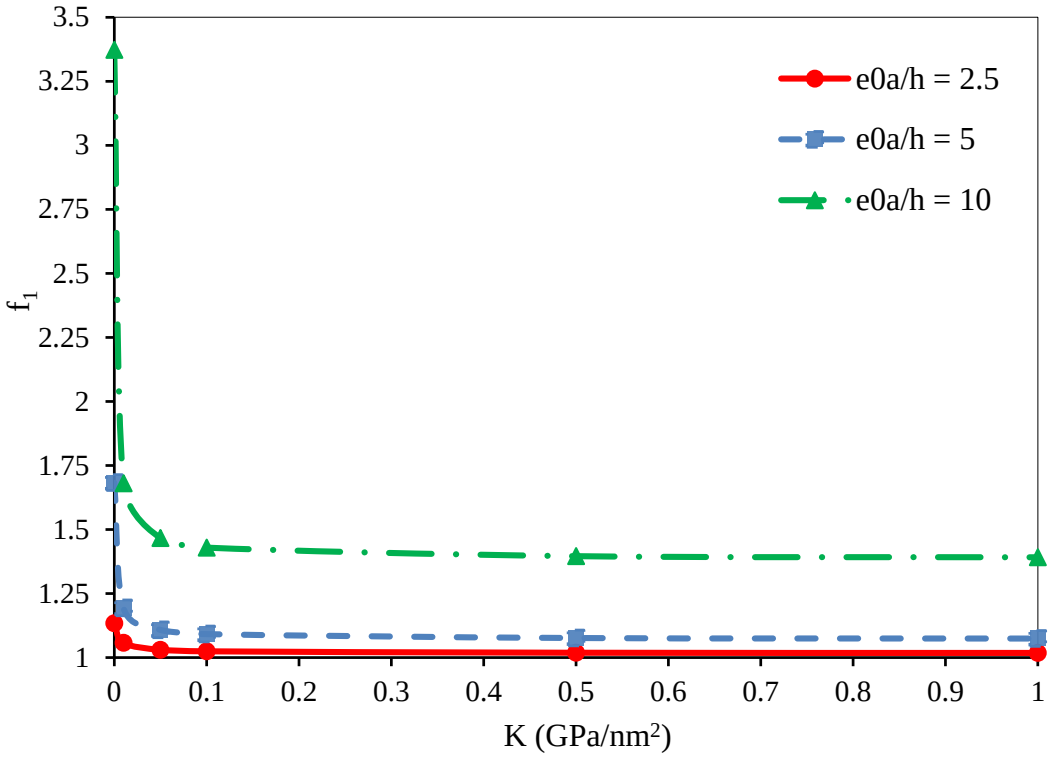

(a)

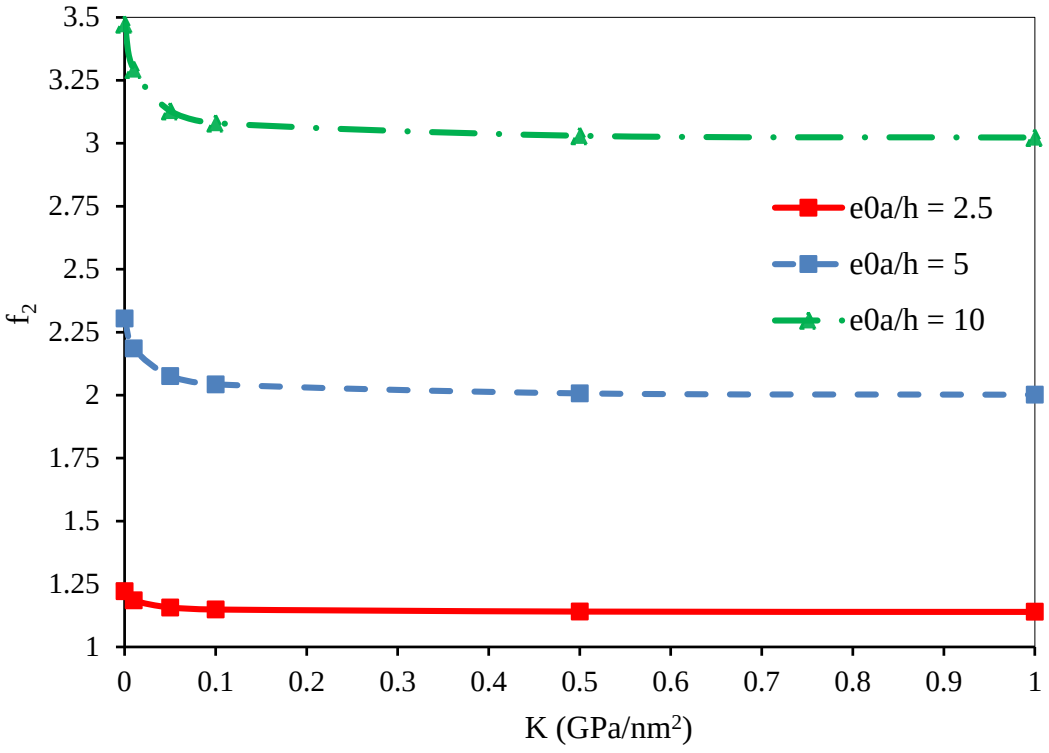

(b)

Fig. 9. The effect of K coefficient on (a) first (b) second natural frequency for different values of dimensionless nonlocal parameter $(e_0 a)/h$

10. Conclusions and remarks

In this study, we made an effort to achieve the deformations and natural frequencies of the SARS-CoV-2 virus. For this purpose, the virus is simulated by a spherical structure, and mathematical equations are obtained by theories of mechanics. Since the virus has nanometer dimensions and also its material structure is assumed viscoelastic, the nonlocal elasticity theory has been used to derive the governing equations. Applying loads and vibrations with natural frequencies can be considered as a treatment method. The results can be categorized and expressed as follows:

- By applying mechanical load, deformations can be created in the structure of the SARS-CoV-2 virus that cause its destruction.

- The applying time of the load should be extended to create maximum deformation in the structure.
- The internal materials of the virus, which play the role of an elastic foundation, reduce the deformations created in it.
- The first and second natural frequencies are to create resonance in the range of $3\ GHz < f_1 < 4\ GHz$ and $7\ GHz < f_2 < 25\ GHz$.
- Considering the viscoelastic property as well as nonlocal analysis causes the values of the obtained results to be more than those of the classical results.
- If the radius of the virus is about $100\ nm$ (average radius of SARS-CoV-2 virus), the distance between classical and nonlocal results is insignificant.

Declaration of Competing Interest

The authors declare that they have no known competing financial interests or personal relationships that could have appeared to influence the work reported in this paper.

References

Aoe, T. 2019. Pathological Aspects of COVID-19 as a Conformational Disease and the Use of Pharmacological Chaperones as a Potential Therapeutic Strategy, https://doi.org/10.3389/fphar.2020.01095.

Assiri, A. et al., 2013. Hospital Outbreak of Middle East Respiratory Syndrome Coronavirus, New England J Med. 369, 407–416. https://doi.org/10.1056/nejmoa1306742.

Audoly, B., Hutchinson, J.W., 2020. Localization in spherical shell buckling, J. Mech. Phys. Solids 136, 103720. https://doi.org/10.1016/j.jmps.2019.103720.

Bansal, A.S., Bradley, A.S., Bishop, K.N., Kiani-Alikhan, S., Ford, B., 2012. Chronic fatigue syndrome, the immune system and viral infection, Brain, Behavior, and Immunity 26, 24–31. https://doi.org/10.1016/j.bbi.2011.06.016.

Beigel, J.H., et al., 2020. Remdesivir for the Treatment of Covid-19 — Final Report, New England J. Med. 383, 1813–1826. https://doi.org/10.1056/nejmoa2007764.

Bills, K.B., et al., 2019. Targeted Subcutaneous Vibration With Single-Neuron Electrophysiology As a Novel Method for Understanding the Central Effects of Peripheral Vibrational Therapy in a Rodent Model, Dose-Response 17, 1–7, https://doi.org/10.1177/1559325818825172.

Boni, C., Royer-Carfagni, G., 2021. A nonlocal elastica inspired by flexural tensegrity, Int. J. Eng. Sci. 158, 103421. https://doi.org/10.1016/j.ijengsci.2020.103421.

Boyd-Brewer, C., 2003. Vibroacoustic Therapy: Sound Vibrations in Medicine, Altern. Complement. Ther. 9, 257–263. https://doi.org/10.1089/107628003322490706.

Cruz-González, O.L., Rodríguez-Ramos, R., Otero, J.A. Ramírez-Torres, A., Penta, R., Lebon, F., 2020. On the effective behavior of viscoelastic composites in three dimensions, Int. J. Eng. Sci. 157, 103377. https://doi.org/10.1016/j.ijengsci.2020.103377.

Dai, H., et al., 2020. Erratum: Bispecific CAR-T cells targeting both CD19 and CD22 for therapy of adults with relapsed or refractory B cell acute lymphoblastic leukemia, J. Hematol. Oncol. 13, 1–11. https://doi.org/10.1186/s13045-020-00878-2.

Dastjerdi, S., Abbasi, M., 2020. A new approach for time-dependent response of viscoelastic graphene sheets embedded in visco-Pasternak foundation based on nonlocal FSDT and MHSDT theories, Mech. Time-Depend. Mater. 24, 329–361. https://doi.org/10.1007/s11043-019-09424-1.

Dastjerdi, S., Akgöz, B., 2019. On the statics of fullerene structures, Int. J. Eng. Sci. 142, 125-144. https://doi.org/10.1016/j.ijengsci.2019.06.002.

Dastjerdi, S., Akgöz, B., Civalek, Ö., 2020. On the effect of viscoelasticity on behavior of gyroscopes, Int. J. Eng. Sci. 149, 103236. https://doi.org/10.1016/j.ijengsci.2020.103236.

Dastjerdi, S., Akgöz, B., Civalek, Ö., 2021a. On the shell model for human eye in Glaucoma disease, Int. J. Eng. Sci. 158, 103414. https://doi.org/10.1016/j.ijengsci.2020.103414.

Dastjerdi, S., Malikan, M., Dimitri, R., Tornabene, F., 2021b. Nonlocal elasticity analysis of moderately thick porous functionally graded plates in a hygro-thermal environment, Compos. Struct. 255, 112925. https://doi.org/10.1016/j.compstruct.2020.112925.

Dastjerdi, S., Naeijian, F., Akgöz, B., Civalek, Ö., 2021c. On the mechanical analysis of microcrystalline cellulose sheets, Int. J. Eng. Sci. 166, 103500. https://doi.org/10.1016/j.ijengsci.2021.103500.

de Kleer, J., 1986. An assumption-based TMS, Artif. Intel. 28, 127–162. https://doi.org/10.1016/0004-3702(86)90080-9.

de Wit, E., et al., 2020. Prophylactic and therapeutic remdesivir (GS-5734) treatment in the rhesus macaque model of MERS-CoV infection, Proc. National Academy Sci. USA. 117, 6771–6776. https://doi.org/10.1073/pnas.1922083117.

Diniz, P., Shomura, K., Soejima, K., Ito, G., 2002. Effects of Pulsed Electromagnetic Field (PEMF) Stimulation on Bone Tissue Like Formation Are Dependent on the Maturation Stages of the Osteoblasts, Bioelectromagnet. 23, 398–405, https://doi.org/10.1002/bem.10032.

Domenyuk, D.A., Zelensky, V.A., Rzhepakovsky, I.V., Anfinogenova, O.I., Pushkin, S.V., 2018. Application of Laboratory and X-Ray Gentral Studies un Early Diagnostics of Metabolic Disturbances of Bone Tissue in Children with Autoimmune Diabetes Mellitus, Entomol. Appl. Sci. Lett. 5, 1–12.

Eremeyev, V. A., Ivanova, E. A., Morozov, N. F., 2015. On free oscillations of an elastic solids with ordered arrays of nano-sized objects, Continuum Mech. Thermodyn. 27, 583–607. https://doi.org/10.1007/s00161-014-0343-z

Eringen, A.C., Edelen, D.G.B., 1972. On nonlocal elasticity, Int. J. Eng. Sci. 10, 233-248. https://doi.org/10.1016/0020-7225(72)90039-0.

Eringen, A.C., 1983. On differential equations of nonlocal elasticity and solutions of screw dislocation and surface waves, J. Appl. Phys. 54, 4703-4707, https://doi.org/10.1063/1.332803.

Eringen, A.C. Nonlocal continuum field theories, Springer, New York, 2002.

Fu, C.L.A., et al., 2013. The effect of early whole-body vibration therapy on neuromuscular control after anterior cruciate ligament reconstruction: A randomized controlled trial, Am. J. Sports Med. 41, 804–814. https://doi.org/10.1177/0363546513476473.

Gautret, P., et al., 2020. Hydroxychloroquine and azithromycin as a treatment of COVID-19: results of an open-label non-randomized clinical trial, Int. J. Antimicrob. Agents 56, 105949. https://doi.org/10.1016/j.ijantimicag.2020.105949.

Ghayesh, M. H., 2019. Viscoelastic dynamics of axially FG microbeams, Int. J. Eng. Sci. 135, 75-85. https://doi.org/10.1016/j.ijengsci.2018.10.005.

Heireche, H., Tounsi, A., Benzair, A., 2008. Scale effect on wave propagation of double-walled carbon nanotubes with initial axial loading, Nanotechnol. 19, 185703. https://doi.org/10.1088/0957-4484/19/18/185703.

Ivanovska, I. L., de Pablo, P. J., Ibarra, B., Sgalari, G., MacKintosh, F. C., Carrascosa, J. L., Schmidt, C. F., Wuite, G. J. L., 2004. Bacteriophage capsids: Tough nanoshells with complex elastic properties. Proc. Natl. Acad. Sci. U S A. 101, 7600-7605. https://doi.org/10.1073/pnas.0308198101.

Jalaei, M. H., Civalek, Ö., 2019. On dynamic instability of magnetically embedded viscoelastic porous FG nanobeam, Int. J. Eng. Sci. 143, 14-32, https://doi.org/10.1016/j.ijengsci.2019.06.013.

Jin, Y.H. et al., 2020. A rapid advice guideline for the diagnosis and treatment of 2019 novel coronavirus (2019-nCoV) infected pneumonia (standard version), Med. J. Chinese People's Lib. Army 45, 1–20. https://doi.org/10.11855/j.issn.0577-7402.2020.01.01.

Karami, B., Shahsavari, D., Janghorban, M., 2019. On the dynamics of porous doubly-curved nanoshells, Int. J. Eng. Sci. 143, 39-55. https://doi.org/10.1016/j.ijengsci.2019.06.014.

Kudin, K. N., Scuseria, G. E., Yakobson, B. I., 2001. C_2F, BN, and C nanoshell elasticity from *ab initio* computations, Phys. Rev. 64, 235406. https://doi.org/10.1103/PhysRevB.64.235406.

Li, A., Wang, B., Yang, Sh., 2021. On some basic aspects of flexoelectricity in the mechanics of materials, Int. J. Eng. Sci. 166, 103499. https://doi.org/10.1016/j.ijengsci.2021.103499.

Ma, Y., Nolte, R.J.M., Cornelissen, J.J.L.M., 2012. Virus-based nanocarriers for drug delivery, Adv. Drug Deliv. Rev. 64, 811–825. https://doi.org/10.1016/j.addr.2012.01.005.

Malikan, M., Eremeyev, V.A., 2020. On the Dynamics of a Visco–Piezo–Flexoelectric Nanobeam, Symmetry 12, 643. https://doi.org/10.3390/sym12040643.

Malikan, M., Uglov, N.S., Eremeyev, V.A., 2020. On instabilities and post-buckling of piezomagnetic and flexomagnetic nanostructures, Int. J. Eng. Sci. 157, 103395. https://doi.org/10.1016/j.ijengsci.2020.103395.

Malikan, M., Krasheninnikov, M., Eremeyev, V. A., 2020. Torsional stability capacity of a nano-composite shell based on a nonlocal strain gradient shell model under a three-dimensional magnetic field, Int. J. Eng. Sci. 148, 103210. https://doi.org/10.1016/j.ijengsci.2019.103210.

Mirabelli, C., et al., 2020. Morphological cell profiling of SARS-CoV-2 infection identifies drug Repurposing candidates for COVID-19, BioRxiv, https://doi.org/10.1101/2020.05.27.117184.

Mirtskhulava, M.B., Tsibadze, D.A., Sibashvili, G.S., Barnabishvili, N.O., Kvachakidze, M.G., 1995. Vliianie magnitnogo polia na raspredelenie virusa grippa v organakh [The effect of a magnetic field on the distribution of the influenza virus in organs], Vopr Kurortol Fizioter Lech Fiz Kult, 2, [Russian].

Murmu, T., Pradhan, S.C., 2009. Thermo-mechanical vibration of a single-walled carbon nanotube embedded in an elastic medium based on nonlocal elasticity theory, Comp. Mater. Sci. 46, 854-869. https://doi.org/10.1016/j.commatsci.2009.04.019.

Pawluk, W., 2020. Coronavirus, Immunity and Use of Pulsed Electromagnetic Fields (PEMF's), J. Med. Clin. Res. Rev. 4, 1-8.

Pica, F., Serafino, A., Divizia, M., Donia, D., Fraschetti, M., Sinibaldi-Salimei, P., Giganti, M.G., Volpi, A., 2006. Effect of extremely low frequency electromagnetic fields (ELF-EMF) on Kaposi's sarcoma-associated herpes virus in BCBL-1 cells, Bioelectromagnet. 27 226-232. https://doi.org/10.1002/bem.20198.

Prajapat, M., et al., 2020. Drug for corona virus: A systematic review, Indian J. Pharmacol. 52, 56. https://doi.org/10.4103/ijp.IJP_115_20.

Sim, L.C., Yeo, W.H., Purbolaksono, J., Saw, L.H., Tey, J.Y., 2021. Analytical solution of thermo-mechanical stresses of multi-layered hollow spherical pressure vessel, Int. J. Pres. Vessel. Pip. 191, 104355. https://doi.org/10.1016/j.ijpvp.2021.104355.

Sirsi, S.R., Borden, M.A., 2014. State-of-the-art materials for ultrasound-triggered drug delivery. Adv. Drug Deliv. Rev. 72, 3–14. https://doi.org/10.1016/J.ADDR.2013.12.010.

Stephanidis, B., Adichtchev, S., Gouet, P., McPherson, A., Mermet, A., 2007. Elastic Properties of Viruses, Biophys. J. 93, 1354-1359, https://doi.org/10.1529/biophysj.107.109033.

Stoll, G., Pol, J., Soumelis, V., Zitvogel, L., Kroemer, G., 2018. Impact of chemotactic factors and receptors on the cancer immune infiltrate: a bioinformatics study revealing homogeneity and heterogeneity among patient cohorts, OncoImmunol. 7, 1–13. https://doi.org/10.1080/2162402X.2018.1484980.

Şahin, A.R., 2020. 2019 Novel Coronavirus (COVID-19) Outbreak: A Review of the Current Literature, Eur. J. Med. Oncol. 4, 1–7. https://doi.org/10.14744/ejmo.2020.12220.

Şimsek, M., 2011. Forced vibration of an embedded single-walled carbon nanotube traversed by a moving load using nonlocal Timoshenko beam theory, Steel Compos. Struct. 11, 59-76. https://doi.org/10.12989/scs.2011.11.1.059**.**

Velavan, T.P., Meyer, C.G., 2020. The COVID-19 epidemic, Trop. Med. Int. Health 25, 278–280. https://doi.org/10.1111/tmi.13383.

Weiss, S.R., Navas-Martin S., 2005. Coronavirus Pathogenesis and the Emerging Pathogen Severe Acute Respiratory Syndrome Coronavirus. Microbiol. Mol. Biol. Rev. 69, 635–664. https://doi.org/10.1128/MMBR.69.4.635-664.2005.

Xu, X., Karami, B., Shahsavari, D., 2021. Time-dependent behavior of porous curved nanobeam, Int. J. Eng. Sci. 160, 103455. https://doi.org/10.1016/j.ijengsci.2021.103455.

Yan, D., Pezzulla, M., Reis, P.M., 2020. Buckling of pressurized spherical shells containing a through-thickness defect, J. Mech. Phys. Solids 138, 103923. https://doi.org/10.1016/j.jmps.2020.103923.

Yin, S., Li, B., Feng, X.Q., 2021. Bio-chemo-mechanical theory of active shells, J. Mech. Phys. Solids 152, 104419. https://doi.org/10.1016/j.jmps.2021.104419.

Ziemann, U., 2004. TMS and drugs, Clin. Neurophysiol. 115, 1717–1729. https://doi.org/10.1016/j.clinph.2004.03.006.